01 Jan 2017

Monotonic and Cyclic Response of Single Shear Cold-Formed Steel-to-Steel and Sheathing-to-Steel Connections

American Iron and Steel Institute

research report

Monotonic and Cyclic Response of Single Shear Cold-Formed Steel-to-Steel and Sheathing-to-Steel Connections

Report RP17-2

January 2017

American Iron and Steel Institute

DISCLAIMER

The material contained herein has been developed by researchers based on their research findings and is for general information only. The information in it should not be used without first securing competent advice with respect to its suitability for any given application. The publication of the information is not intended as a representation or warranty on the part of the American Iron and Steel Institute or of any other person named herein, that the information is suitable for any general or particular use or of freedom from infringement of any patent or patents. Anyone making use of the information assumes all liability arising from such use.

VIRGINIA POLYTECHNIC INSTITUTE
AND STATE UNIVERSITY

The Charles E. Via, Jr. Department
of Civil and Environmental Engineering
Blacksburg, VA 24061

Structural Engineering and Materials

Monotonic and Cyclic Response of Single Shear Cold-Formed Steel-to-Steel and Sheathing-to-Steel Connections

by
Fannie Tao
Graduate Research Assistant

Aritra Chatterjee
Graduate Research Assistant

Cristopher D. Moen, Ph.D., P.E.
Graduate Research Advisor

Report No. CE/VPI-ST-16-01

January 2017

Table of Contents

Abstract

Monotonic and cyclic backbone load-deformation response models for single shear steel-to-steel and plywood, oriented-strand board, and gypsum board sheathing to cold-formed steel screw-fastened connections are developed with support from an experimental program. Connection strength, stiffness, and the probability of screw shear failure are correlated to fastener bearing strength of the two connected plies. Cyclic strength and stiffness degradation was negligible. Cyclic excursions resulted in increased connection stiffness from the screw bearing hardening the ply material and locking in the plies.

1 Introduction

Monotonic and cyclic backbone load-deformation response models are developed with steel-to-steel and sheathing-to-steel experiments in this report to provide the capability to simulate connections for performance-based design (e.g., FEMA P695 analysis) of cold-formed steel framed buildings. Screw fasteners serve as the primary connectors in light steel framing (Figure 1a), and their discrete behavior defines lateral and gravity system response (Figure 1b). Whole building seismic analysis, i.e., modeling every cold-formed steel stud, track, shear wall, floor diaphragm, and fastener (Figure 1c), becomes feasible when connection response, including strength and stiffness degradation and energy dissipation, is accurately predicted.

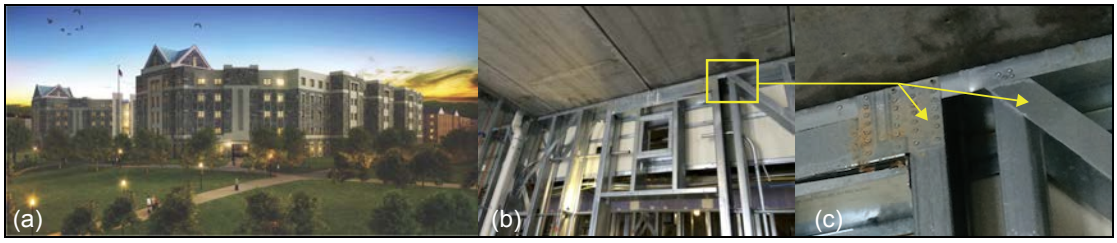

Figure 1: Cold-formed steel framing in (a) 5-story Virginia Tech residence hall constructed with (b) panelized load-bearing framing connected by (c) self-drilling screw fasteners

Extensive test data on cold-formed steel fasteners is available (Peköz 1990), and most of these tests focus on monotonic ultimate strength and failure limit states. For example, it is well documented that a fastener will tilt at the connection if the moment created by the single shear eccentricity cannot be resisted by the plies which occurs when both steel plies are relatively thin. If one of both plies are relatively thick, then fastener bearing is the controlling strength limit state. These limit states are represented in codes and standards such as Section E4 in AISI-S100-12.

More recent work has focused on documenting complete fastener load-deformation response, including cyclic strength and stiffness degradation of typical cold-formed steel framing connections (Peterman et al. 2014, Ayhan and Schafer 2016, Moen at al. 2016). Initial stiffness and post-peak response is known for different fastener head types (Haus and Moen 2014), and steps have been taken to parameterize the monotonic backbone response (Moen et al. 2014, Pham and Moen 2015). Cyclic strength and stiffness degradation at the fastener level can also be considered in whole building models with newly coded pinching material models (Ding 2015) that accommodate accurate nonlinear dynamic time history analyses (Niari et al. 2012, Bian et al. 2014, Ngo 2014, Fülöp and Dubina 2006).

This report derives monotonic and cyclic load-deformation backbone and pinching parameter models for steel-to-steel and sheathing-to-steel single-shear cold-formed steel screw-fastened connections, where the sheathing is oriented strand board (OSB), Structural 1 plywood, and paper-laminated gypsum. These models will be used as inputs for pushover and cyclic seismic simulations of light steel framed subsystems (shear walls, diaphragms) and whole building analysis (Padilla 2015), where the connections are inputted as nonlinear springs or hysteretic elements. Building serviceability calculation and retrofit procedures, for example, those outlined by ASCE 41-13 (Pekelnicky and Poland 2012), can also be developed from the models, where connection stiffness at a specific fastener load is required.

2 Single shear screw-fastened connection experimental program

The experimental program documented in this report represents the single-shear screw-fastened connections commonly found in cold-formed steel light-framed buildings. The steel-to-steel screw-fastened connections cover load-bearing framing while the sheathing tests (OSB, plywood, and gypsum) characterize roofing, diaphragm, and exterior and interior wall connections. Specimens were constructed with two plies (Ply 1 being the ply in contact with the fastener head) and a single fastener. Both monotonic and cyclic loadings were applied.

2.1 Screw-fastened connection test matrix

The test matrices for steel-to-steel and sheathing-to-steel are shown in Table 1 and Table 2, respectively. For the steel-to-steel tests, six steel ply thicknesses and three fastener types were varied. The nominal ply thicknesses, 18, 33, 43, 54, 68, and 97, are in thousands of an inch (mils) (SFIA 2016), and the fasteners used in this study were #8, #10, and #12 self-drilling, hex-head fasteners. Each combination was subjected to both monotonic and cyclic loading with three trials each, totaling 222 tests.

Table 1: Steel-to-steel fastener test matrix

Ply 2 (steel in mils)	*Ply 1 (steel in mils)*																	
	18			***33***			***43***			***54***			***68***			***97***		
	#8	*#10*	*#12*	*#8*	*#10*	*#12*	*#8*	*#10*	*#12*	*#8*	*#10*	*#12*	*#8*	*#10*	*#12*	*#8*	*#10*	*#12*
18	-	-	-	-	-	-	-	-	-	3	3	3	-	-	-	-	-	-
33	-	-	-	3	3	3	3	3	3	3	3	3	3	3	3	3	3	3
43	-	-	-	-	-	-	3	3	3	-	-	-	-	-	-	-	-	-
54	3	3	3	-	-	-	3	3	3	-	-	-	-	-	-	-	-	-
68	-	-	-	-	-	-	3	3	3	-	-	-	-	-	-	-	3	3
97	-	-	-	-	-	-	3	3	3	-	-	-	-	-	-	-	3	3

For the sheathing-to-steel tests, three types of sheathing at three thicknesses, five steel ply thicknesses, and four fastener types were varied. The focus of the sheathing experimental study was sheathing of medium-thickness (14.9 mm for the OSB, 14.7 mm for the Structural 1 plywood, and 12.6 mm for the gypsum). Additional sheathing tests (sheathing of thin-thickness with a thin steel ply and a small fastener, sheathing of thick-thickness with a thick steel ply and a large fastener) were also considered to anchor the limits of generalized parameter trends introduced later in this report. The fasteners used in the OSB and plywood tests were #8, #10, and #12 self-drilling, flat-head fasteners. For the gypsum tests, two different #6 bugle-head fasteners were used, depending on the thickness of the steel in the combination. The same procedure of monotonic and cyclic loading with three trials each was applied to the sheathing tests, which resulted in 186 total tests.

Table 2: Sheathing-to-steel fastener test matrix

Ply 2 (steel in mils)	*Ply 1 (sheathing in mm)*													
	OSB					***Plywood***					***Gypsum***		
	11.6	***14.9***			***17.9***	***11.4***	***14.7***			***17.3***	***9.54***	***12.6***	***16.1***
	#8	*#8*	*#10*	*#12*	*#12*	*#8*	*#8*	*#10*	*#12*	*#12*	*#6*	*#6*	*#6*
33	3	3	3	-	-	3	3	3	-	-	3	3	-
43	-	3	3	-	-	-	3	3	-	-	-	3	-
54	-	3	3	3	-	-	3	3	3	3	-	3	3
68	-	-	3	3	-	-	-	3	3	3	-	-	-
97	-	-	3	3	3	-	-	3	3	3	-	-	-

Ply 1 varies between steel and sheathing while Ply 2 is consistently a steel ply. The test naming convention defines the thicknesses of Ply 1 (or designation of Ply 1 for sheathing) and Ply 2, fastener size, loading type (M=monotonic, C=cyclic), and trial number within a test series. The

designation of the sheathing ply is “1” for the thinnest, “2” for the medium thickness, and “3” for the thickest. For a steel-to-steel example, ‘4354-10-M2’ is the test combination with a 43 Ply 1 (t_1=43 thousandths of an inch=1.11 mm), 54 Ply 2 (t_2=54 thousandths of an inch=1.43 mm), a #10 hex-head fastener, and the second of three monotonic loading trials. For a sheathing-to-steel example, ‘P233-8-C1’ is the test combination with a 14.7 mm-thick plywood Ply 1, 33 Ply 2 (t_2=33 thousandths of an inch=0.90 mm), a #8 flat-head fastener, and the first of three cyclic loading trials.

2.2 Test setup

The schematic of the test setup for the experiments is shown in Figure 2. A stiff steel base anchors the test setup. Two aluminum fixtures with a 102 mm by 102 mm window support the specimen on three sides, and this test setup was refined over multiple iterations (Corner 2014, Okasha 2004). When the specimen is loaded axially, there is a moment that develops at the fastener from the loads on the plies and the distance between them causes the plies to separate. Although this is a common occurrence in a standard connection test (AISI S905-13), it is inconsistent with typical framing connection behavior, where studs and tracks provide enough flexural stiffness to prevent ply separation (Haus and Moen 2014). To counter this separation effect, the window was developed to provide lateral restraint and keep the plies in contact.

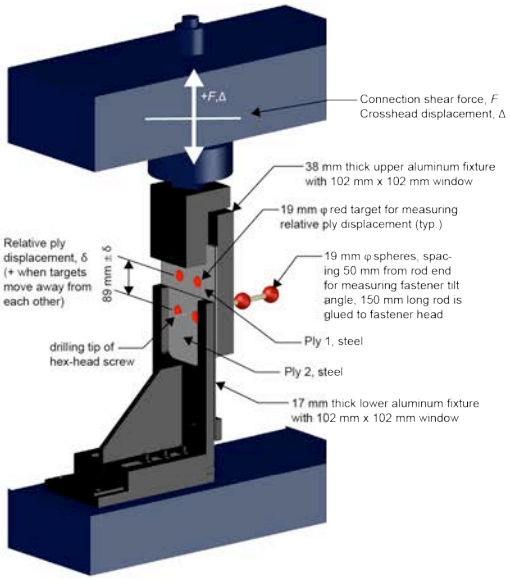

Figure 2: Single shear screw-fastened connection test setup

2.3 Specimen construction, installation, and fastener details

Each specimen consists of two plies and a single fastener. The dimensions of the plies and location of the fastener is depicted in Figure 3. The typical installation process was to drive the fastener from Ply 1 into Ply 2 at the center of the overlapping section, install the specimen between the aluminum fixtures with 13 mm diameter bolts (three in the top aluminum fixture, two in the bottom aluminum fixture), and tighten the bolts. The load cell reading was zeroed before bolt tightening to measure the pretension or precompression force that sometimes developed in the fastener specimen. The drilled bolt hole and bolt size are both 13 mm in diameter, resulting in a bearing connection that minimized ply slip in the grips during loading.

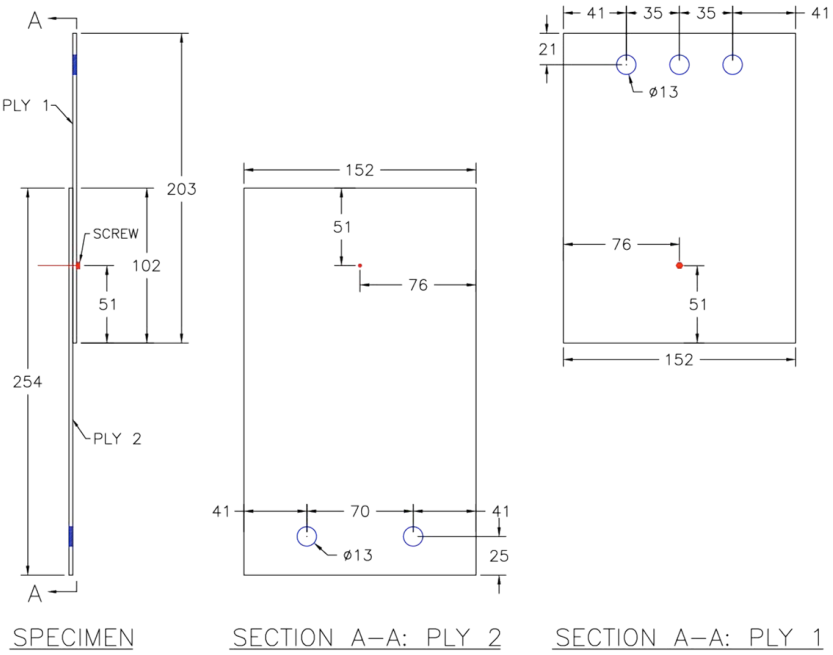

Figure 3: Specimen dimensions (in mm) and construction

Table 3 documents the properties of all the fasteners that were used in this study. The steel-to-steel #8 fasteners were provided by ELCO Construction Products, and the remaining fasteners were provided by Simpson Strong-Tie. The length for the steel-to-steel fasteners were the same, and the length for the sheathing-to-steel fasteners were closely matched based on material availability. As the fastener size increases, there is an increase in head diameter, major thread diameter (out-to-out), D, and fastener shear strength, F_{ss}. Figure 4 shows illustrations of the fasteners used for (a) steel-to-steel, (b) wood sheathing-to-steel, (c) gypsum-33-mil steel, and (d) gypsum-to-43, 54-mil steel.

Table 3: Fastener types, dimensions, and details

Fastener	*Product #*	*Head Type*	*Coating*	*Length (mm)*	*Head diameter (mm)*	*Major thread diameter, D (mm)*	*Fss (kN)*
Steel-to-steel #8	EDA285	Hex	Clear-zinc	25	8.3	4.20	4.9
Steel-to-steel #10	X1S1016	Hex	Clear-zinc	25	10.2	4.74	8.2
Steel-to-steel #12	X1S1214	Hex	Clear-zinc	25	10.2	5.40	11.1
Gypsum-to-33-mil steel #6	DWF158PS	Bugle	Gray-phosphate	41	8.1	3.45	5.6
Gypsum-to-43, 54-mil steel #6	DWFSD158PS	Bugle	Yellow-zinc	41	8.0	3.45	5.6
Wood sheathing-to-steel #8	PPSD11516S0818	Flat	Yellow-zinc	49	8.1	4.14	7.5
Wood sheathing-to-steel #10	PPSD134S1016	Flat	Yellow-zinc	44	8.3	4.67	8.9
Wood sheathing-to-steel #12	PPSD134S1214	Flat	Yellow-zinc	44	11.6	5.41	11.9

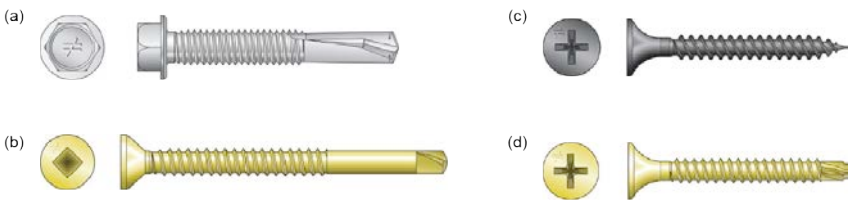

Figure 4: Fasteners used in experiments: (a) steel-to-steel, (b) wood sheathing-to-steel, (c) gypsum-to-33-mil steel, and (d) gypsum-to-43, 54-mil steel

2.4 Test measurements and instrumentation

Relative displacement between the plies, δ in Figure 2, was measured with an optical non-contact measurement system developed and validated at Virginia Tech to an accuracy of ± 0.10 mm (Pham and Moen 2015). During each test, a Microsoft Lifecam cinema HD 720p video camera recording at 30 frames per second was used to video record and track four red sticker targets (two on each ply, see Figure 2 for target locations). The video is inputted into the custom Matlab code (provided in Appendix A), which uses the Matlab Computer Vision System Toolbox (Matlab 2015). The code performs a frame-by-frame analysis and records the centroidal coordinates (*x* and *y*) and areas of each recognized target and the timestamp for every frame. It outputs a .mat file containing all frame information.

Figure 5 shows a screenshot of the frame-by-frame analysis. Four red targets are detected, and the centroids, areas, and times are recorded in a vector. The relative displacement is then calculated by averaging the target area (in pixels) for the first 50 frames and using a ratio between this value and the measured target area (285 mm^2) to convert the vertical distance between targets from pixels to mm, i.e.

$$\frac{\delta(mm)}{\delta(pixels)} = \sqrt{\frac{Area(mm)}{AverageArea(pixels)}} \tag{1}$$

Figure 5: Matlab frame-by-frame post-processing of the displacement video camera

The connection force, *F*, was measured with the test machine 150 kN load cell (accuracy of ± 0.10 kN), and the crosshead displacement, *Δ*, was measured with the test machine internal LVDT (accuracy of ± 0.10 mm). The connection force data was matched to the relative ply displacement using the timestamps from the test machine and the video files. The crosshead displacement was used to validate the accuracy of the optical non-contact measurement system and to apply the monotonic and cyclic loading protocols.

2.5 Specimen material properties

ASTM standards were followed to obtain material properties for the steel, OSB, plywood, and sheathing. The properties of interest were the thickness (*t*), ultimate (peak) stress (f_u), and modulus of elasticity (*E*) to be used with the models discussed later in Section 4.

2.5.1 Steel stress-strain properties

The steel plies used in this experimental study were provided by ClarkDietrich Building Systems out of their Sparrows Points, MD facility. Three tensile coupons per steel ply were tested in accordance with ASTM E8M (ASTM 2004) except for the 97-mil ply, which had inaccurate displacement readings before yield for the third coupon and was subsequently discarded. The average (μ) and coefficient of variation (c_v) of base metal thickness (t) from five measurements along each tensile coupon, yield stress (f_y), ultimate stress (f_u), and elongation at fracture from three tensile coupon tests are summarized in Table 4.

Table 4: Steel ply material properties for Delivery 1

Ply	***t* (mm)**		***f_y (MPa)***		***f_u (MPa)***		**% elongation at fracture**	
	μ	c_v	μ	c_v	μ	c_v	μ	c_v
18	0.50	0.03	294	0.03	361	0.05	23.1	0.11
33	0.90	0.01	325	0.03	376	0.02	34.1	0.03
43	1.11	0.01	590	0.01	615	0.01	7.4	0.07
54	1.43	0.00	393	0.01	493	0.00	24.4	0.10
68	1.80	0.00	390	0.04	510	0.03	20.3	0.10
97	2.56	0.00	379	0.00	505	0.02	21.9	0.07

A second batch of steel was required to complete the tests (again coming from ClarkDietrich), and their properties are summarized in Table 5.

Table 5: Steel ply material properties for Delivery 2

Ply	***t* (mm)**		***f_y (MPa)***		***f_u (MPa)***		**% elongation at fracture**	
	μ	c_v	μ	c_v	μ	c_v	μ	c_v
33	0.86	0.01	330	0.02	408	0.02	32.6	0.02
43	1.12	0.01	306	0.01	377	0.01	33.3	0.06
54	1.44	0.00	381	0.02	512	0.01	25.1	0.01
68	1.83	0.00	374	0.05	489	0.02	21.1	0.07
97	2.52	0.00	333	0.01	475	0.01	26.4	0.02

The stress-strain curves for the steel are included in Appendix B. The batch of steel used in each test are listed in Tables B1 and B2, alongside general test parameters described in Section 4.1. All specimens exhibited a typical stress-strain curve with a yield plateau followed by strain hardening except for the 43 plies which fractured at 60% less elongation and had a yield stress about 65% higher and an ultimate stress about 35% higher than the other specimens.

2.5.2 Sheathing

Dowel bearing strength tests were conducted in accordance with ASTM D5764 (ASTM 2013) to obtain the yield stress (f_y), ultimate stress (f_u), and modulus of elasticity (E) of the OSB,

Structural 1 plywood, and gypsum. A full-hole setup was used with 50.8 mm by 76.2 mm test specimens with a 9.5 mm diameter hole. A Grade 8, 9.5 mm diameter steel dowel was placed through the hole, and the specimen is loaded uniformly from the top at a constant loading rate of 1 mm/min. The test is stopped at the first occurrence of either a 10% drop from the maximum load or a crosshead displacement of 10.2 mm. Outer ply wood grains were oriented parallel to the applied load.

To obtain the modulus of elasticity and yield stress, a straight line was fit to the initial linear region of the load-deformation curve and offset by 5% of the fastener diameter (9.5 mm). The slope of the fit line was taken as the modulus of elasticity, and the load at which the offset line intersects the load-deformation curve was taken as the yield load. The yield stress was calculated by dividing the yield load by the dowel bearing area. The ultimate stress was taken as the maximum load recorded divided by the dowel bearing area. A summary of the sheathing material properties and the corresponding statistics are shown in Table 6.

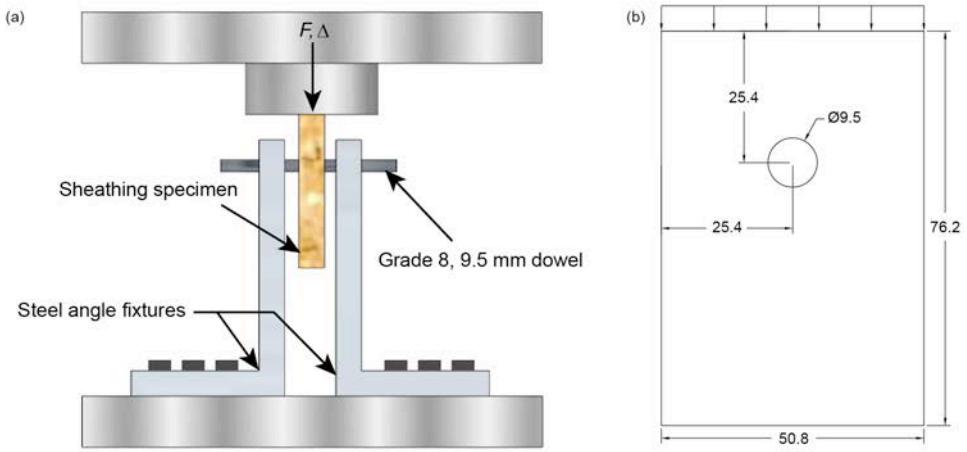

Figure 6: (a) Dowel bearing test setup and (b) sheathing specimen dimensions for bearing tests

Table 6: Sheathing material properties

Sheathing		***Sample size, n***	***t* (mm)**		***f_y (MPa)***		***f_u (MPa)***		***E (MPa)***	
			μ	c_v	μ	c_v	μ	c_v	μ	c_v
OSB	11.6 mm	10	11.6	0.02	29.6	0.25	33.4	0.18	606	0.15
	14.9 mm	5	14.9	0.03	32.9	0.05	40.9	0.17	699	0.07
	17.9 mm	5	17.9	0.01	22.7	0.28	33.8	0.17	678	0.15
Plywood	11.4 mm	5	11.4	0.01	32.6	0.15	41.0	0.26	523	0.10
	14.7 mm	6	14.7	0.02	47.9	0.12	56.1	0.12	908	0.21
	17.3 mm	5	17.3	0.00	43.8	0.14	51.4	0.14	875	0.18
Gypsum	9.54 mm	5	9.54	0.00	8.40	0.12	10.3	0.06	240	0.12
	12.6 mm	5	12.6	0.00	5.10	0.10	6.80	0.04	142	0.12
	16.1 mm	5	16.1	0.01	8.80	0.07	10.9	0.04	177	0.27

The load-deformation curves for the sheathing are included in Appendix C. Most specimens followed a similar load-deformation curve with yielding and failure occurring soon after hitting peak load. As expected, the gypsum board was observed to be weaker than OSB and plywood, and plywood was the strongest.

2.6 Specimen loading

Monotonic tests were loaded at a constant displacement rate of Δ=0.025 mm/sec (Okasha 2004). The cyclic loading protocol is adopted from the FEMA 461 quasi-static cyclic deformation-controlled testing protocol (FEMA 2007) as shown in Figure 7, which was developed to obtain fragility data and hysteretic response characteristics of building components for which damage is best predicted by imposed deformations. The protocol defines two cycles at equal displacement amplitude per step and a 40% displacement amplitude increase per step, $\Delta_i=1.4\Delta_{i-1}$.

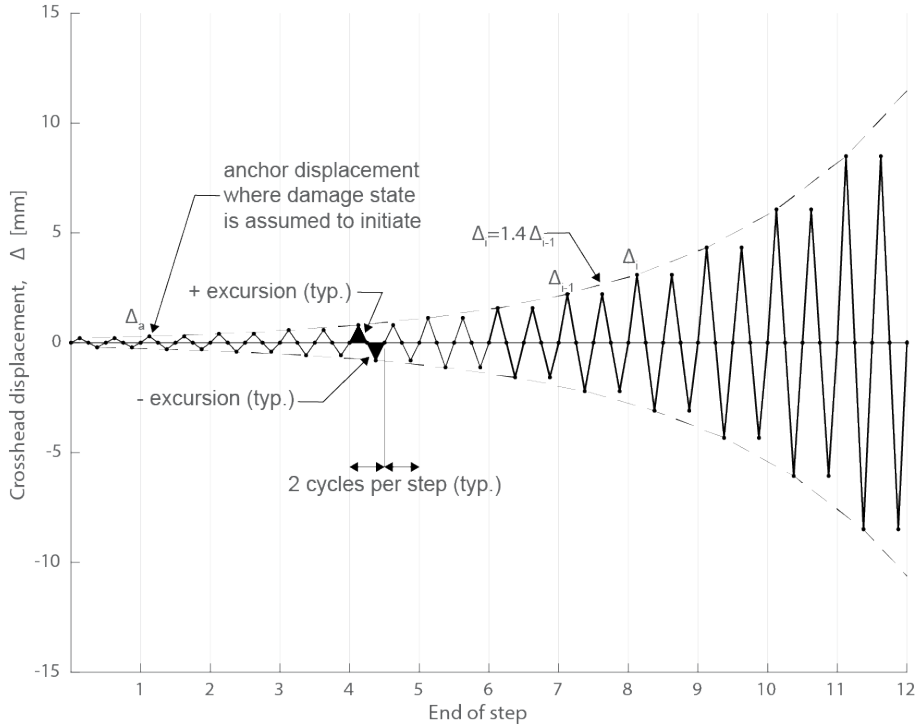

Figure 7: Cyclic fastener loading protocol, shown here for fastener configuration 3333-8

For the experiments described in this report, the cyclic loading protocol was anchored at the third cycle (beginning of second step). Although FEMA recommends performing six deformation cycles before reaching the first damage limit state, this was not practical for these connections tests due to plasticity initiating at lower load levels from ply bearing deformation. The crosshead displacement anchor point, Δ_a, is assumed to represent the initiation of the fastener damage state (Pham and Moen 2015). Assuming crosshead and relative ply displacements are equivalent, the anchor displacement, Δ_a, is calculated as the predicted relative displacement corresponding to $0.40F_c$ in the elastic region, i.e., $\Delta_a=\delta_a=0.4F_c/K_e$, where F_c is the peak (cap) load and K_e is the elastic stiffness of the monotonic response shown in Figure 8.

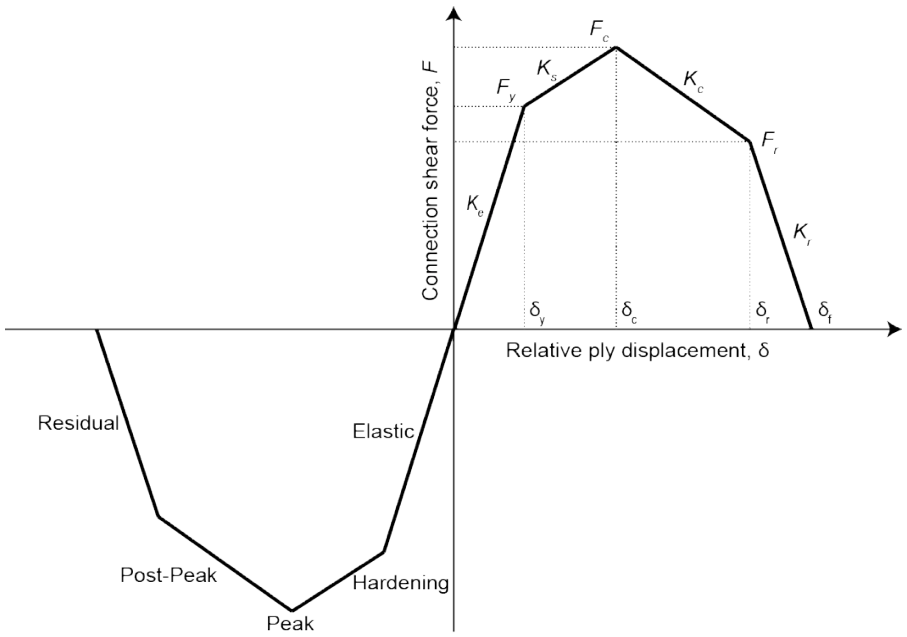

Figure 8: Backbone curve nomenclature

3 Fastener load-deformation monotonic and cyclic response

3.1 Fastener load-deformation backbone nomenclature

Backbone curves are used to characterize monotonic and cyclic fastener load-deformation responses for developing hysteretic models with strength and stiffness degradation. The backbone configuration (Figure 8) is inspired by the Ibarra-Medina-Krawinkler model (2005), and each curve consists of five regions: elastic, hardening, peak, post-peak, and residual. Each region is defined by its associated load and displacement points ((F_y, δ_y), (F_c, δ_c), (F_r, δ_r), and (0, δ_f)) and related stiffnesses (slopes) K_e, K_s, K_c, and K_r.

3.2 Fastener load-deformation backbone construction procedure

Monotonic backbone construction was performed by visually selecting (F_c, δ_c) as the first peak load after hardening, then visually selecting (Fy, δ_y) to match the elastic and hardening slopes, K_e and K_s, respectively. The point (F_r, δ_r) is obtained so that the post-peak backbone segment from (F_c, δ_c) to (F_r, δ_r) is a linear fit (i.e., the average) of the tested response, and then δ_r is calculated by equating the energy dissipation of the tested load-displacement curve and backbone response. The backbone of the positive cyclic response (+F in Figure 2) was obtained by first identifying the response outline with the Matlab Boundary command (Matlab 2015) with the 'shrink factor'=1 and then following the same monotonic backbone construction procedure. Backbones are constructed for each ply combination and for both monotonic and (positive) cyclic loadings. Tables of all backbone parameters (steel-to-steel, OSB-to-steel, plywood-to-steel, gypsum-to-steel) and the statistics based on the average of the three trials are included in Appendix D, where M represents the monotonic loading, and C represents the positive cyclic loading.

3.3 Fastener load-deformation response for steel-to-steel specimens

An example set of steel-to-steel backbones is shown in Figure 9. This ply combination failed through fastener screw shear, which is evident in the large drop in load at small displacement changes. Depending on the ply combination, the specimen failed in fastener screw shear, bearing, or fastener screw pull-out after tilting.

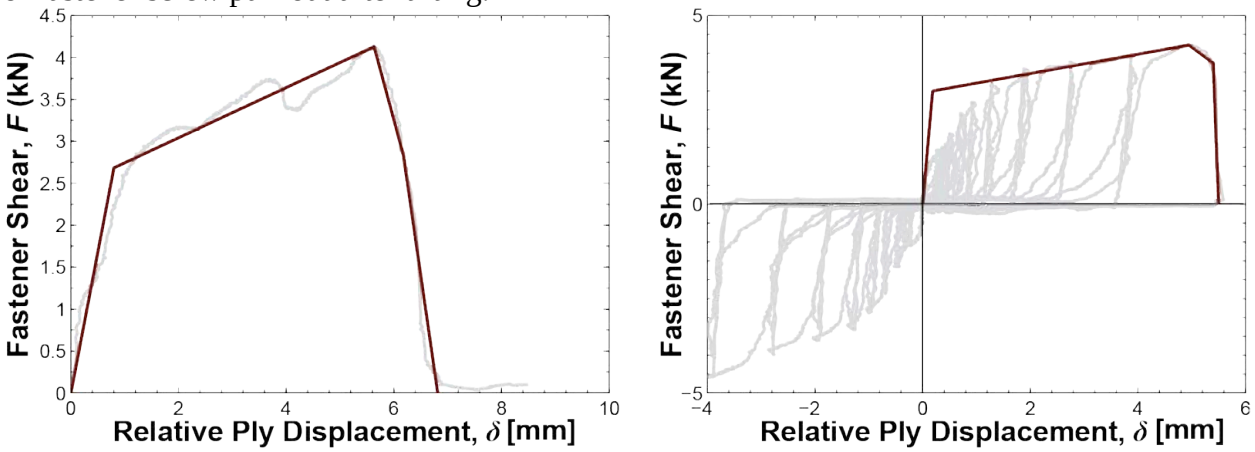

Figure 9: Backbones for fastener configuration 5433-8-1: (a) monotonic and (b) cyclic loading

3.4 Fastener load-deformation response for OSB-to-steel specimens

An example set of OSB-to-steel backbones is shown in Figure 10. With the OSB combinations, fastener screw pull-out and fastener screw shear were the predominant modes of failure. For the fastener screw pull-out mode, the fastener tilts at the initiation of loading and bears through the wood until it pulls out of the steel ply. For fastener screw shear, the two plies are stiff enough to resist the tilting of the fastener head, and eventually, the fastener shears. The areas where load drops and immediately increases, as seen in the monotonic load-deformation response in Figure 10(a), represent the OSB splintering as the fastener bears through.

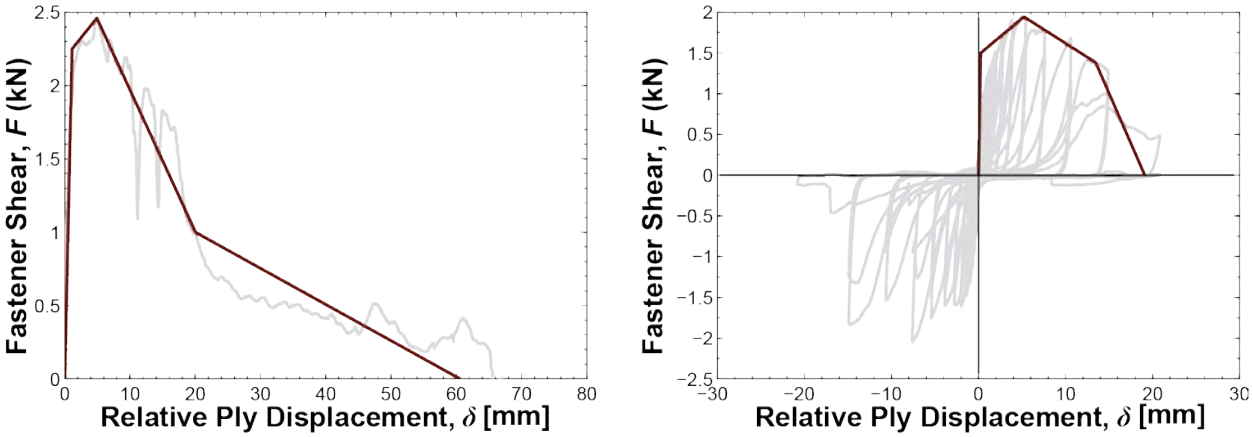

Figure 10: Backbones for fastener configuration O133-8-3: (a) monotonic and (b) cyclic loading

3.5 Fastener load-deformation response for plywood-to-steel specimens

An example set of plywood-to-steel specimens is shown in Figure 11. Plywood and OSB are similar in the way the combinations failed (fastener shear or fastener pull-out). However, in terms of strength, it is clear from Figure 10 and Figure 11 that plywood is stronger, reaching peak loads more than two times as high.

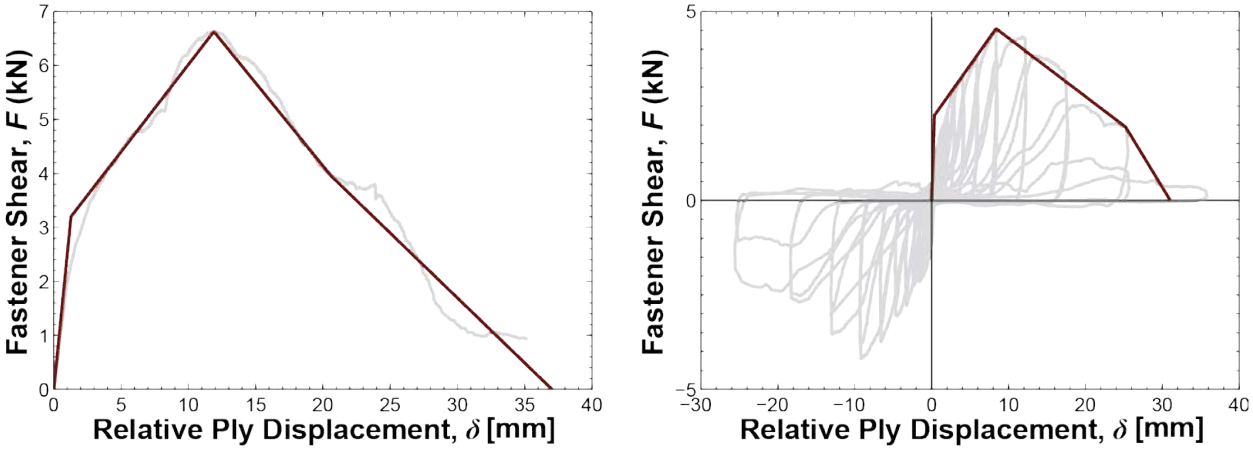

Figure 11: Backbones for fastener configuration P254-12-2: (a) monotonic and (b) cyclic loading

3.6 Fastener load-deformation response for gypsum-to-steel specimens

An example set of gypsum-to-steel backbones is shown in Figure 12. Because gypsum was weak in comparison with the other materials, most of the failures were from the fastener bearing through the gypsum ply. The fastener did not tilt in these combinations as it did in the OSB and plywood specimens because of how weak gypsum was in comparison with the steel ply and fastener. The point where the load drops almost vertically is when the fastener has torn through the gypsum. Under cyclic loading, the fastener bears in both directions and shows minimal strength degradation within excursions.

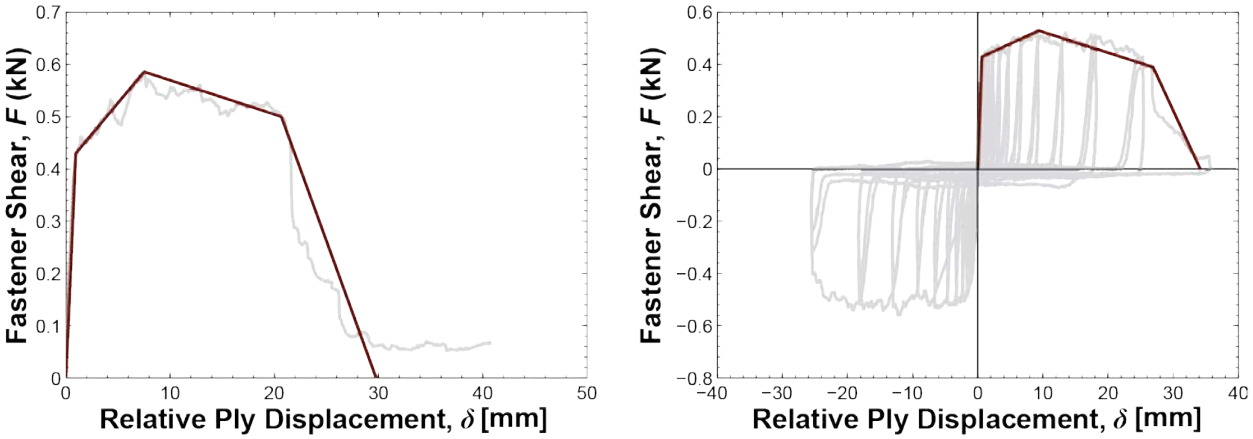

Figure 12: Backbones for fastener configuration G254-6-3: (a) monotonic and (b) cyclic loading

4 Fastener load-deformation monotonic and cyclic backbone parameters

4.1 Fastener load-deformation backbone parameter calculation procedure

Based on the tested trends and observations, models are proposed for the backbone loads (F_y, F_c, F_r) and stiffnesses (K_e, K_s, K_c, and K_r). The fastener load model is $F_{[y,c,r]}=\alpha\psi^{\beta}F_{ss} \leq F_{ss}$, where $\psi=[F_{ss}/(t_1DF_{u1})][(F_{ss}/t_2DF_{u2})]$ and F_{ss} is the fastener shear strength (typically determined experimentally by manufacturers). The fastener stiffness model is $K_{[e,s,c,r]}=\alpha\psi^{\beta}K_a$, where $K_a=[1/(E_1t_1)+1/(E_2t_2)]^{-1}$ which is the axial stiffness of the two plies treated as springs in series assuming a rigid fastener connection, and E_1 and E_2 are the ply elastic moduli. The values for ψ obtained for each test are listed in Tables B1 and B2 in Appendix B. The parameters α and β, shown in Table 7-Table 11 are calculated with the Matlab function *fminsearch* minimizing the difference in error between test and model. The backbone model framework accommodates high strength steel plies (Rogers and Hancock 1999), OSB, plywood, and gypsum and is limited to $\psi \leq$ 90. Model parameters are proposed for all the experiments. The monotonic and cyclic backbone load and stiffness models can be used to calculate δ_y, δ_c, δ_r, and δ_g in Figure 8, e.g., $\delta_y=F_y/K_e$.

For some of the ply combinations, there was a shear failure of the fastener as a result of thick plies and small fasteners (small ψ). With a fastener shear failure, the post-peak backbone segments do not follow the backbone configuration in Figure 8. Once the specimen is loaded to its peak and the fastener shears, the load vertically drops and plateaus at a negligible amount of load (i.e., Figure 9). This introduces high values for K_c, making it harder to fit a trend. For this

reason, a backbone model with no post-peak segments was proposed for specimens failing in fastener shear, and the probability of fastener screw shear was modeled (Section 4.6). These specimens were excluded from the following F_r, K_c, and K_r models.

Fastener load-deformation backbone parameters: steel-to-steel and sheathing-to-steel connections in Table 7 contains the backbone model parameters for all the steel-to-steel and sheathing-to-steel combinations, and Figure 13 plots the models with the trend parameters. Ply bearing strengths, t_1Df_{u1} and t_2Df_{u2}, were found to be key contributors to the strength and stiffness of the connection. Decreasing either of the ply thicknesses or ultimate stresses (i.e., having a weak ply) reduces the strength and stiffness, which can be seen in any of the backbone models. Increasing fastener sizes from #8 to #12 increases the strength and stiffness because the bearing stress and associated deformation in each ply decreases. The yielding load, F_y, and peak (cap) load, F_c, experience minimal cyclic degradation (Figure 13a and b) as the fasteners repeatedly bear on the plies, and it is hypothesized that the positive cyclic (C+) elastic connection stiffness (K_e) is approximately double the monotonic stiffness (Figure 13d) because of material accumulation from bearing deformation.

Table 7: Steel and sheathing backbone model parameters and test-to-predicted statistics

Backbone parameter	*Loading*	*Trend parameters* α	β	*Test/Predicted* μ	c_v
F_y	monotonic	1.26	-0.62	1.00	0.39
	cyclic	1.32	-0.66	1.00	0.35
F_c	monotonic	1.66	-0.56	1.00	0.33
	cyclic	1.65	-0.57	1.00	0.31
F_r	monotonic	1.32	-0.69	1.00	0.41
	cyclic	0.91	-0.52	1.00	0.38
K_e	monotonic	0.51	-0.52	1.00	1.02
	cyclic	1.08	-0.50	1.00	0.99
K_s	monotonic	0.031	-0.50	1.00	0.87
	cyclic	0.050	-0.65	1.00	1.23
K_c	monotonic	-0.080	-0.76	1.00	1.15
	cyclic	-0.080	-0.80	1.00	1.08
K_r	monotonic	-0.17	-0.95	1.00	2.39
	cyclic	-0.21	-0.95	1.00	1.50

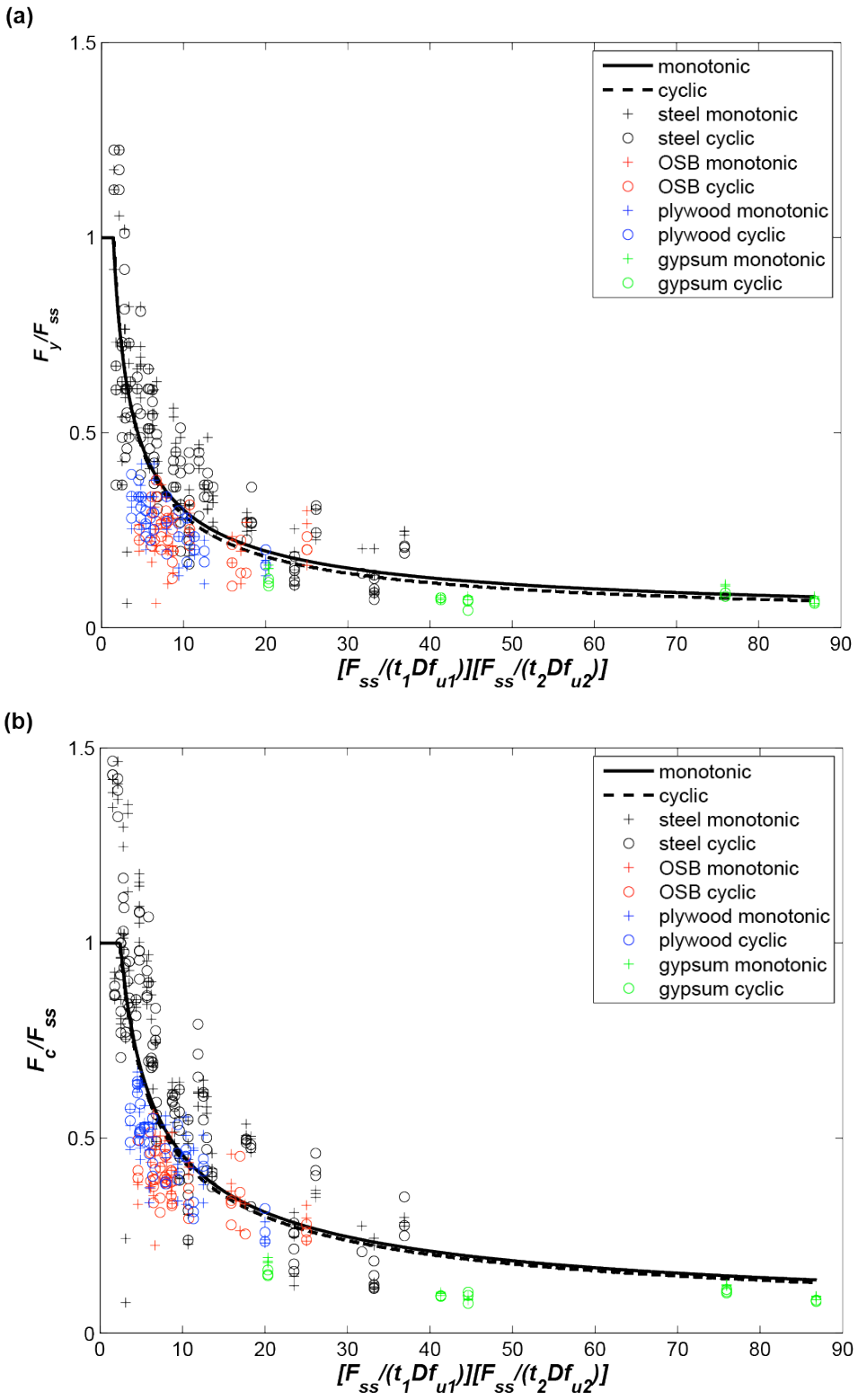

Figure 13: Steel and sheathing fastener backbone models: (a) F_y, (b) F_c, (c) F_r, (d) K_e, (e) K_s, (f) K_c, and (g) K_r

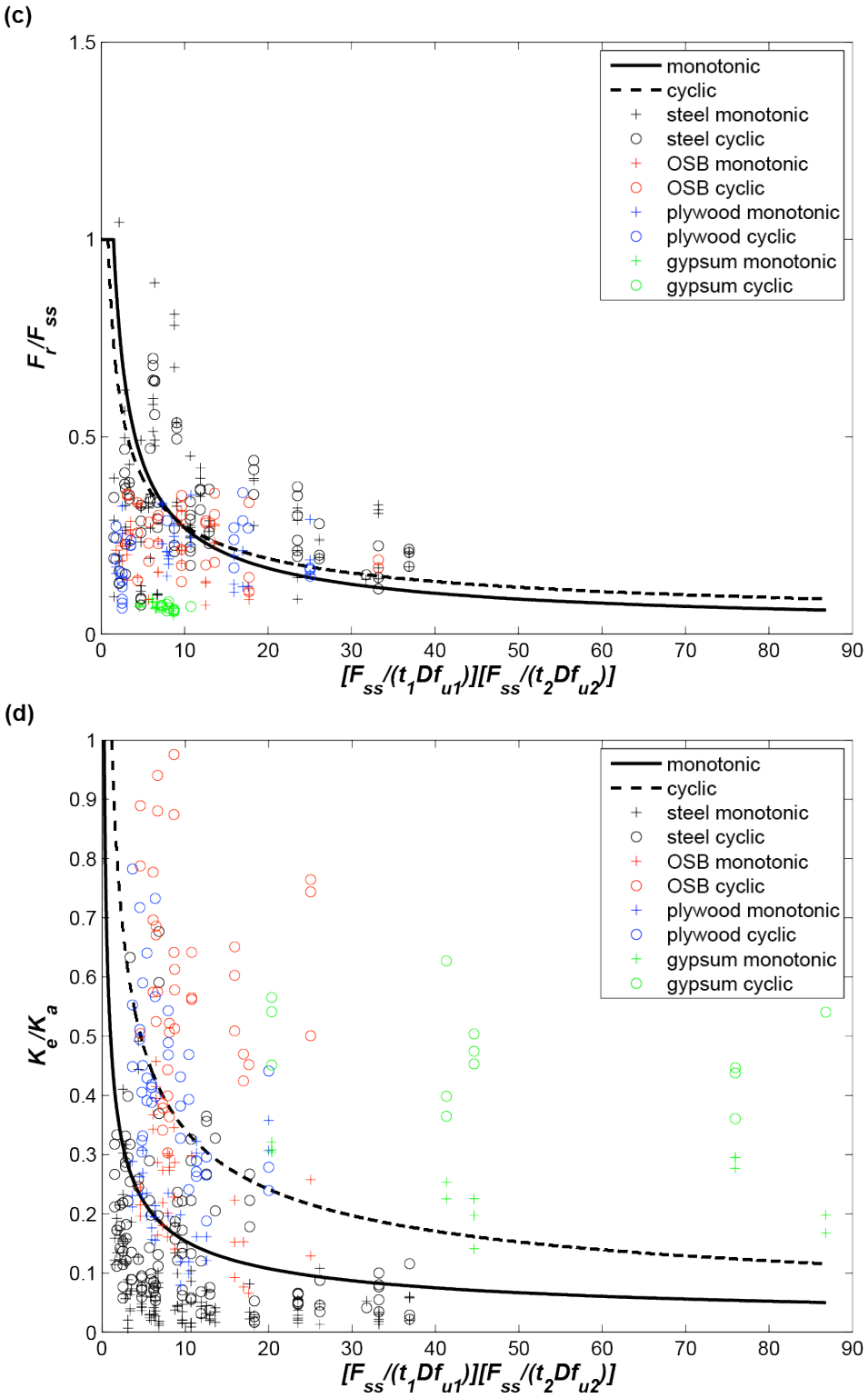

Figure 13: Steel and sheathing fastener backbone models: (a) F_y, (b) F_c, (c) F_r, (d) K_e, (e) K_s, (f) K_c, and (g) K_r

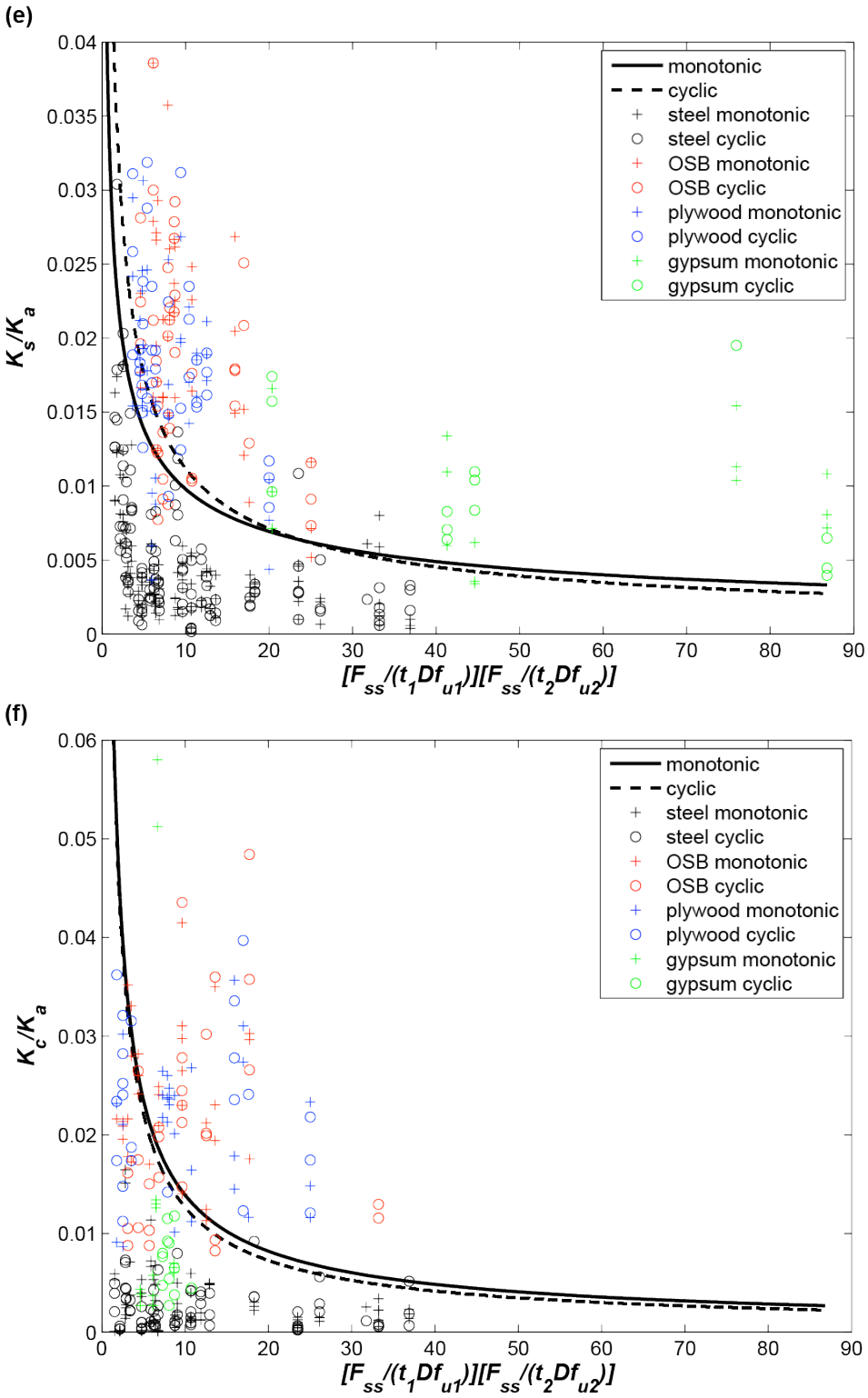

Figure 13: Steel and sheathing fastener backbone models: (a) F_y, (b) F_c, (c) F_r, (d) K_e, (e) K_s, (f) K_c, and (g) K_r

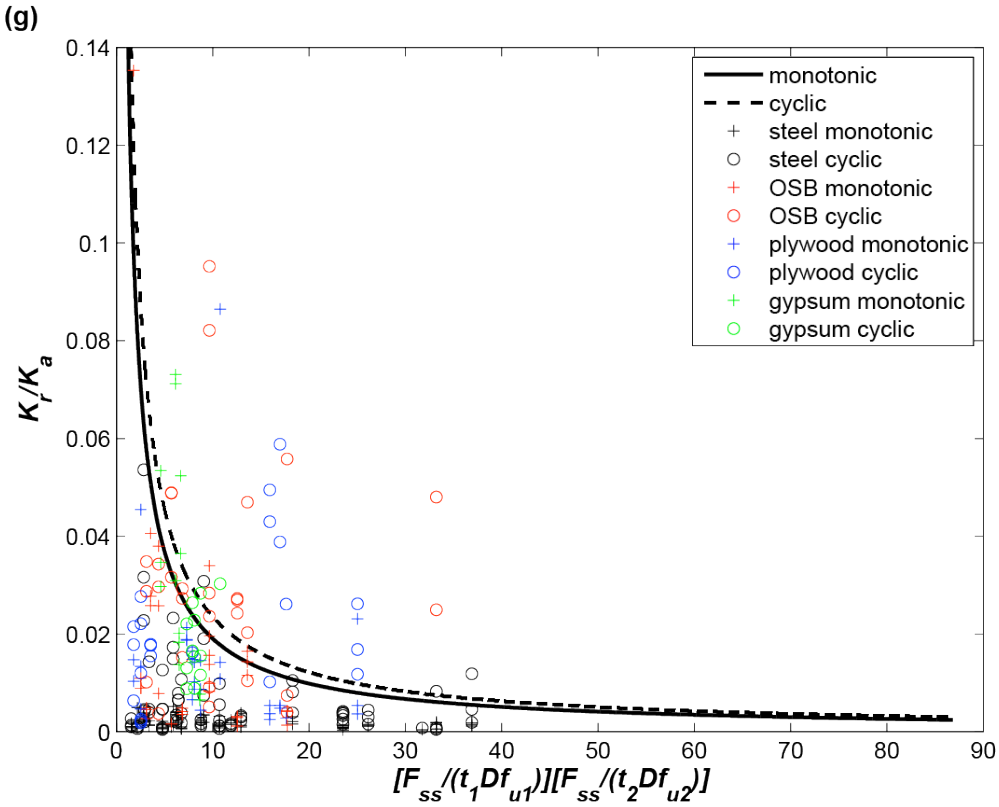

Figure 13: Steel and sheathing fastener backbone models: (a) F_y, (b) F_c, (c) F_r, (d) K_e, (e) K_s, (f) K_c, and (g) K_r

4.2 Fastener load-deformation backbone parameters: steel-to-steel connections

Table 8 contains the backbone model parameters for the steel-to-steel combinations. Again, the same trend discussed earlier can be applied to these models as well. There is minimal cyclic degradation, and the cyclic K_e is approximately double the monotonic K_e.

Table 8: Steel backbone model parameters and test-to-predicted statistics

Backbone parameter	*Loading*	*Trend parameters* α	β	*Test/Predicted* μ	c_v
F_y	monotonic	1.20	-0.50	1.00	0.29
	cyclic	1.25	-0.55	1.00	0.28
F_c	monotonic	1.63	-0.48	1.00	0.29
	cyclic	1.59	-0.47	1.00	0.26
F_r	monotonic	2.12	-0.78	1.00	0.30
	cyclic	1.43	-0.63	1.00	0.29
K_e	monotonic	0.27	-0.69	1.00	0.86
	cyclic	0.65	-0.69	1.00	0.80
K_s	monotonic	0.017	-0.69	1.00	0.76
	cyclic	0.025	-0.82	1.00	0.80
K_c	monotonic	-0.012	-0.60	1.00	0.94
	cyclic	-0.010	-0.58	1.00	0.87
K_r	monotonic	-0.0058	-0.48	1.00	0.50
	cyclic	-0.040	-0.77	1.00	1.19

4.3 Fastener load-deformation backbone parameters: OSB-to-steel connections

Table 9 contains the backbone model parameters for the OSB-to-steel combinations. Although there were not as many OSB test specimens as steel, similar trends can be detected. There is an increase in strength and stiffness as the ply bearing strengths increase and a higher cyclic K_e. More cyclic degradation of the F_c is observed which can be a result of the how forces flow through wood grain (i.e., wood splintering) in comparison with a steel ply.

Table 9: OSB backbone model parameters and test-to-predicted statistics

Backbone parameter	*Loading*	*Trend parameters* α	β	*Test/Predicted* μ	c_v
F_y	monotonic	0.36	-0.21	1.00	0.29
	cyclic	0.38	-0.22	1.00	0.23
F_c	monotonic	0.62	-0.20	1.00	0.17
	cyclic	0.64	-0.24	1.00	0.15
F_r	monotonic	0.94	-0.69	1.00	0.23
	cyclic	0.80	-0.50	1.00	0.31
K_e	monotonic	0.56	-0.37	1.00	0.34
	cyclic	0.87	-0.17	1.00	0.28
K_s	monotonic	0.044	-0.36	1.00	0.33
	cyclic	0.033	-0.29	1.00	0.38
K_c	monotonic	-0.047	-0.30	1.00	0.28
	cyclic	-0.044	-0.34	1.00	0.48
K_r	monotonic	-1.11	-2.00	1.00	0.96
	cyclic	-0.10	-0.50	1.00	0.69

4.4 Fastener load-deformation backbone parameters: plywood-to-steel connections

Table 9 contains the backbone model parameters for all the steel-to-steel and sheathing-to-steel combinations. There is an increase in plywood cyclic stiffness when compared with monotonic stiffness, a trend that is not observed in the OSB specimens. It is hypothesized that the plywood compacts more and becomes stiffer under cyclic loading than OSB.

Table 10: Plywood backbone model parameters and test-to-predicted statistics

Backbone parameter	*Loading*	*Trend parameters* α	β	*Test/Predicted* μ	c_v
F_y	monotonic	0.67	-0.48	1.00	0.23
	cyclic	0.68	-0.48	1.00	0.15
F_c	monotonic	0.96	-0.35	1.00	0.17
	cyclic	0.95	-0.37	1.00	0.13
F_r	monotonic	0.54	-0.44	1.00	0.32
	cyclic	0.51	-0.44	1.00	0.35
K_e	monotonic	0.39	-0.30	1.00	0.40
	cyclic	0.98	-0.43	1.00	0.27
K_s	monotonic	0.030	-0.27	1.00	0.35
	cyclic	0.032	-0.28	1.00	0.28
K_c	monotonic	-0.032	-0.20	1.00	0.34
	cyclic	-0.035	-0.20	1.00	0.34
K_r	monotonic	-0.069	-0.75	1.00	1.00
	cyclic	-0.24	-1.19	1.00	0.54

4.5 Fastener load-deformation backbone parameters: gypsum-to-steel connections

Table 11 contains the backbone model parameters for gypsum-to-steel combinations. The number of gypsum specimens was the smallest of all the material types, and it is apparent in the trends. There is minimal correlation between K_e and K_s and fastener parameters and therefore the trends in Table 11 are provided as horizontal lines (i.e., β=0) and there is observed cyclic degradation in F_c and F_y, caused by the gypsum board breaking down as the cyclic loading progresses.

Table 11: Gypsum backbone model parameters and test-to-predicted statistics

Backbone parameter	*Loading*	*Trend parameters* α	β	*Test/Predicted* μ	c_v
F_y	monotonic	0.60	-0.47	1.00	0.26
	cyclic	0.33	-0.36	1.00	0.17
F_c	monotonic	0.73	-0.47	1.00	0.22
	cyclic	0.44	-0.36	1.00	0.13
F_r	monotonic	0.12	-0.13	1.00	0.13
	cyclic	0.12	-0.14	1.00	0.12
K_e	monotonic	0.24	0.00	1.00	0.24
	cyclic	0.50	0.00	1.00	0.20
K_s	monotonic	0.0093	0.00	1.00	0.42
	cyclic	0.013	0.00	1.00	0.68
K_c	monotonic	-0.083	-0.50	1.00	0.93
	cyclic	-0.0071	0.00	1.00	0.42
K_r	monotonic	-0.35	-0.63	1.00	0.60
	cyclic	-0.26	-0.63	1.00	0.40

4.6 Probability of fastener screw shear failure

A model was developed for fastener shear failures, $P_f=\alpha\psi^{\beta}$ where P_f=probability of fastener shear failure (Table 12, Figure 14). This model is useful in high fidelity modeling and system reliability calculations to determine the probability of fastener connections at a specific ψ that will fail in shear. From the model, it can be seen that fastener screw shear failures mostly happen at smaller ψ, which consists of strong plies and weak fasteners. The fastener is the weakest component and thus, shears when loaded.

Table 12: P_f parameters and test-to-predicted statistics

Parameter	*Loading*	*Trend parameters* α	β	*Test/Predicted* μ	c_v
P_f	monotonic	2.22	-1.34	1.00	1.78
	cyclic	2.16	-1.06	1.00	1.81

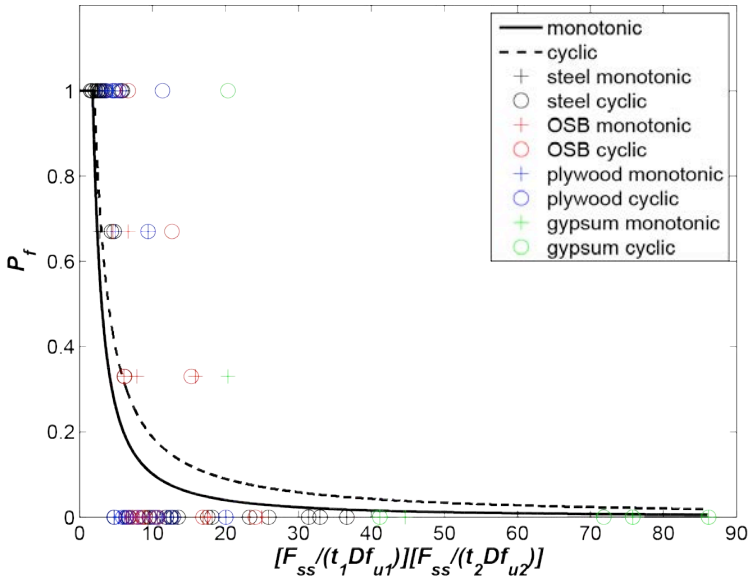

Figure 14: P_f model for all materials

5 Fastener load-deformation pinching model parameters

5.1 Cyclic pinching model definition

The cyclic connection response is characterized as the quadrilinear backbone described in Figure 8, with unloading-reloading response defined by the parameters *rForceP*, *rDispP*, *rForceN*, *rDispN*, *uForceP* and *uForceN*, as discussed in Chatterjee et al. (2017). These parameters which characterize a pinching-type hysteretic model (Lowes et al. 2004, Peterman and Schafer 2013) physically represent ratios of deformations and forces at the onset and termination of reloading/unloading, to the historic maximum and minimum deformations reached during the experiment, as described in Figure 15. The pinching model does not include any strength degradation of the backbone. As the specimen is loaded cyclically its strength softens according to the parameters of the cyclic backbone. This causes the reloading stiffness to degrade (see branch (a) – (b) in Figure 15). The unloading stiffness does not degrade and remains equal to the initial elastic stiffness K_e.

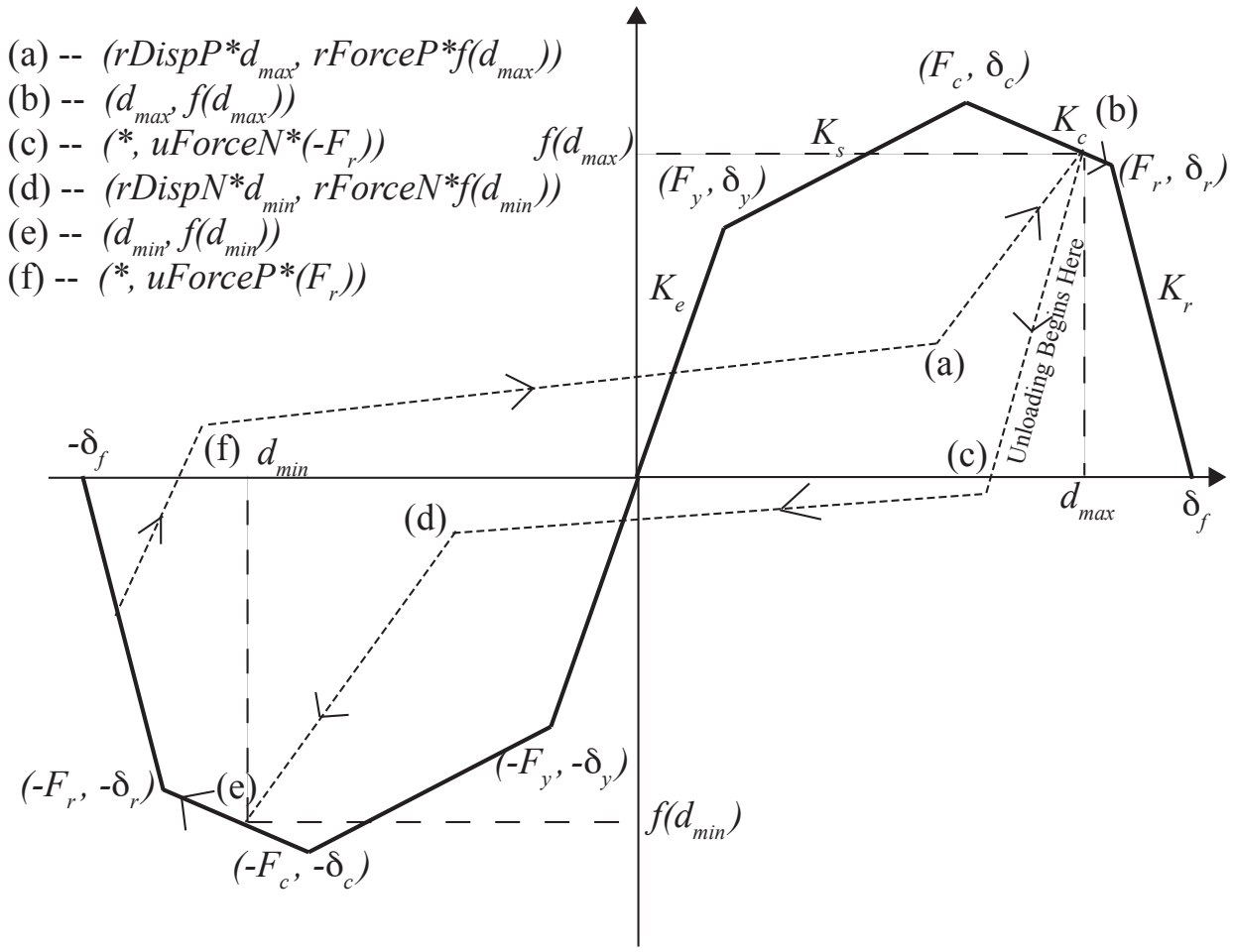

Figure 15 -- Definition of unloading-reloading parameters in cyclic pinching model

This model is preferred to the pinching-hysteretic model described in Ibarra et al. (2005) which was used to model cyclic response in reinforced-concrete columns since it includes non-zero values for *uForceP* and *uForceN* as observed in steel-to-steel connection experiments (see Figure 16 for example), whereas the Ibarra model implicitly assumes these values to be zero.

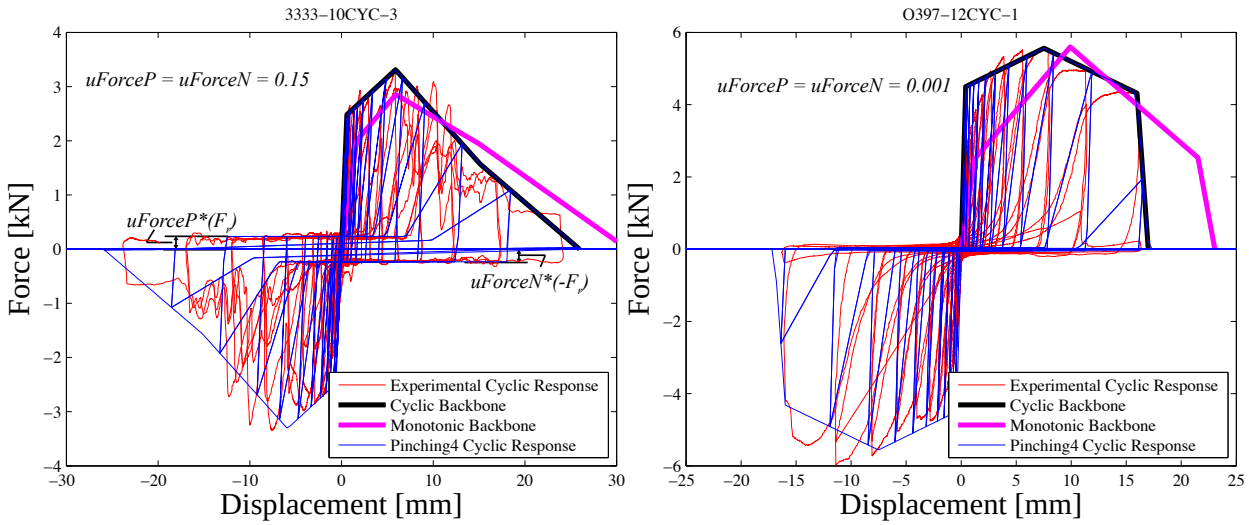

Figure 16 -- Representative cyclic force-deformation relationship showing two limiting cases with *uForceP = uForceN = 0.15* and *uForceP = uForceN = 0.001*

5.2 Cyclic pinching model parameter calculation procedure

The pinching parameters are obtained by minimizing the difference in total energy dissipated experimentally and in the model. The parameters *uForceP* and *uForceN* are set independently outside the optimization loop for stability, and equal 0.001 for OSB-to-steel connections (with the exception of one test case O297-12, see Table 13) which is consistent with Peterman and Schafer (2013), 0.03 for gypsum-to-steel and plywood-to-steel and range from 0.025 to 0.25 for steel-to-steel. The steel-to-steel *uForceP* and *uForceN* parameters functions of ply bearing pressure and deformation. For thin plies connected by a larger screw, load is required to initiate reversal of displacement because the threads stick in the ply, which creates the vertical band about the x-axis shown in Figure 16. As the plies get thicker, the displacement reverses at zero force because there is less local ply deformation, which leads to lower values for *uForceP* and *uForceN* for wood specimens with higher thicknesses. The variation of *uForceP* and *uForceN* with the ply thickness relative to screw size is shown in Figure 17. Once *uForceP* and *uForceN* have been chosen, the remaining parameters *rForceP, rDispP and rForceN, rDispN* are obtained using the MATLAB *fminsearch* routine such that the difference in total hysteretic energy dissipated between the pinching model and the experiments is minimized.

5.3 Cyclic unloading-reloading parameters

Cyclic unloading-reloading parameters for all tests are provided in Table 13. As discussed in Section 5.2, the parameters *uForceP* and *uForceN*, which characterize the width of the vertical band about zero force (Figure 16) are set manually to insure stability in the optimization search. These quantities are related to the ply thicknesses relative to screw diameter by the relationships proposed in Section 4.1 as $uForceP \text{ or } uForceN = \alpha\psi^{\beta}$ and the values for α and β obtained from a fminsearch routine are given in Table 14 with the trendlines plotted in Figure 17. As the ply bearing stress decreases in one or both plies (i.e., as ψ increases), the tendency of the fastener to 'stick' in the weak ply or plies increases, which means leading to larger magnitudes of *uForceP* and *uForceN*.

The parameters *rDispP* and *rDispN* characterize the width of the horizontal band around zero displacement, and are related to hole elongation due to reversing loads, as discussed in Section 5.4.

Table 13 -- Pinching model parametersfor all tests

Test	*rDispP*	*rForceP*	*rDispN*	*rForceN*	*uForceP*	*uForceN*
1854-08	0.906	0.006	0.865	0.000	0.1	0.1
1854-10	0.060	0.013	0.359	0.014	0.2	0.25
1854-12	0.626	0.007	0.729	0.004	0.25	0.25
3333-08	0.054	0.020	0.056	0.018	0.2	0.2
3333-10	0.532	0.009	0.577	0.008	0.15	0.15
3333-12	0.354	0.011	0.362	0.012	0.1	0.1
4333-08	0.551	0.009	0.533	0.009	0.05	0.05
4333-10	0.582	0.009	0.557	0.009	0.075	0.075
4333-12	0.635	0.008	0.655	0.006	0.1	0.075
4343-08	0.853	0.009	0.614	0.006	0.05	0.05
4343-10	0.569	0.010	0.565	0.008	0.05	0.05
4343-12	0.527	0.010	0.546	0.009	0.05	0.05
4354-08	0.514	0.009	0.512	0.010	0.05	0.05
4354-10	0.603	0.009	0.604	0.007	0.05	0.05
4354-12	0.647	0.008	0.669	0.006	0.05	0.05
4368-08	0.628	0.010	0.430	0.008	0.05	0.05
4368-10	0.740	0.005	0.707	0.008	0.05	0.05
4368-12	0.746	0.004	0.789	0.006	0.05	0.05
4397-08	0.558	0.011	0.428	0.010	0.05	0.05
4397-10	0.752	0.005	0.774	0.005	0.05	0.05
4397-12	0.694	0.006	0.658	0.009	0.1	0.1
5418-08	0.725	0.006	0.707	0.005	0.1	0.1
5418-10	0.947	0.003	0.709	0.005	0.1	0.1
5418-12	1.035	0.001	1.211	-0.008	0.1	0.1
5433-08	0.555	0.009	0.528	0.009	0.05	0.05
5433-10	0.672	0.007	0.645	0.008	0.05	0.05
5433-12	0.611	0.009	0.587	0.008	0.05	0.05
6833-08	0.609	0.009	0.483	0.009	0.05	0.05
6833-10	0.722	0.005	0.730	0.007	0.05	0.05
6833-12	0.595	0.008	0.634	0.007	0.05	0.05

9733-08	0.745	0.004	0.709	0.008	0.075	0.075
9733-10	0.811	0.004	0.821	0.004	0.05	0.05
9733-12	0.607	0.004	0.626	0.008	0.1	0.1
9768-10	0.154	0.016	-0.043	0.016	0.025	0.05
9768-12	0.186	0.009	0.357	0.015	0.05	0.05
9797-10	-0.599	0.011	0.826	0.014	0.026	0.025
9797-12	0.144	0.011	0.428	0.013	0.02	0.02
G133-06	0.645	0.010	0.479	0.008	0.03	0.03
G233-06	0.746	0.005	0.752	0.006	0.03	0.03
G243-06	0.823	0.002	0.789	0.007	0.03	0.03
G254-06	0.901	0.001	0.865	0.006	0.03	0.03
G354-06	0.497	0.010	0.453	0.010	0.03	0.03
O133-08	0.562	0.009	0.557	0.008	0.001	0.001
O233-08	0.565	0.010	0.250	0.009	0.001	0.001
O233-10	0.668	0.008	0.638	0.006	0.001	0.001
O243-08	0.474	0.011	0.294	0.012	0.001	0.001
O243-10	0.108	0.016	0.124	0.016	0.001	0.001
O254-08	0.634	0.009	0.626	0.006	0.001	0.001
O254-10	0.584	0.009	0.589	0.008	0.001	0.001
O254-12	0.500	0.009	0.602	0.008	0.001	0.001
O268-10	0.612	0.009	0.605	0.007	0.001	0.001
O268-12	0.539	0.010	0.492	0.009	0.001	0.001
O297-10	0.734	0.007	0.776	0.003	0.001	0.001
O297-12	0.584	0.009	0.572	0.008	0.001	0.001
O397-12	0.753	0.003	0.868	0.006	0.01	0.01
P133-08	0.556	0.009	0.565	0.008	0.03	0.03
P233-08	0.422	0.011	0.432	0.011	0.03	0.03
P233-10	0.636	0.006	0.706	0.008	0.03	0.03
P243-08	0.552	0.009	0.515	0.009	0.03	0.03
P243-10	0.626	0.007	0.594	0.009	0.03	0.03
P254-08	0.527	0.009	0.607	0.007	0.03	0.03
P254-10	0.431	0.010	0.510	0.011	0.03	0.03
P254-12	0.592	0.008	0.618	0.009	0.03	0.03
P268-10	0.726	0.006	0.726	0.005	0.03	0.03

P268-12	0.714	0.004	0.785	0.007	0.03	0.03
P297-10	0.341	0.011	0.466	0.011	0.03	0.03
P297-12	0.688	0.007	0.712	0.004	0.03	0.03
P397-12	0.902	0.002	0.786	0.005	0.03	0.03

Table 14 -- Trend parameters for pinching model *uForce* parameters

Pinching Parameter	Trend Parameters		Test/Predicted	
	α	β	μ	c_v
uForceP	0.017	0.71	1.00	0.47
uForceN	0.017	0.72	1.01	0.48

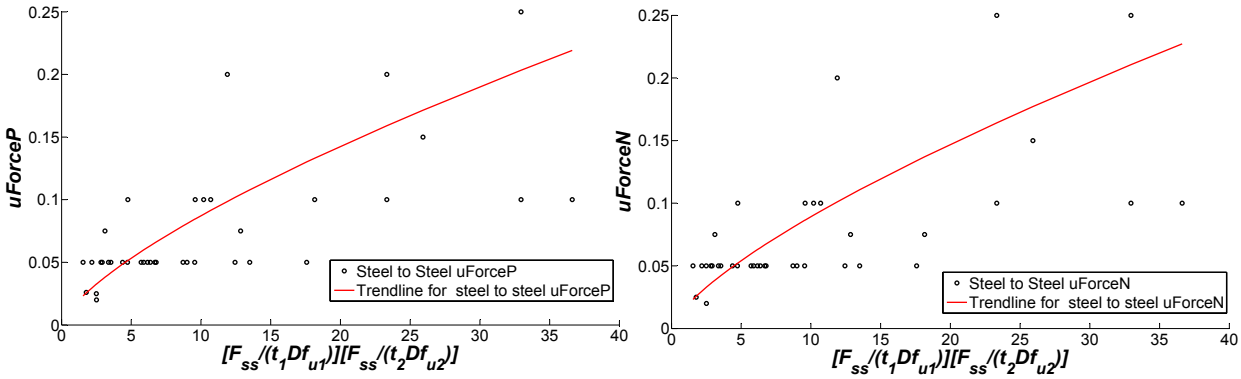

Figure 17 – Trendlines for unloading-reloading parameters *uForceP* and *uForceN*

Table 15 -- Statistics for pinching model *rForce* parameters

	Steel-to-Steel		Steel-to-OSB		Steel-to-Plywood		Steel-to-Gypsum	
	μ	c_v	μ	c_v	μ	c_v	μ	c_v
rForceP	0.0082	0.44	0.0091	0.32	0.0077	0.33	0.0057	0.77
rForceN	0.0081	0.55	0.0081	0.4	0.008	0.28	0.0076	0.24

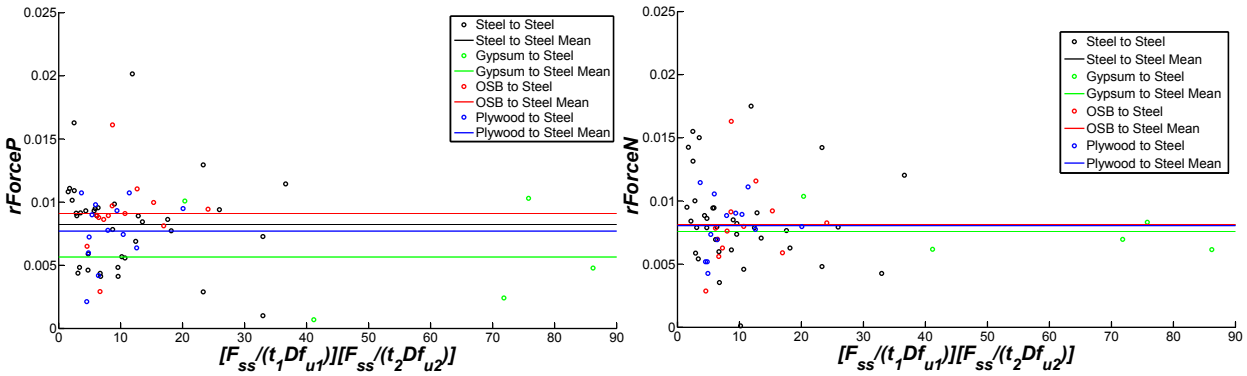

Figure 18 -- Variation in *rForceP* with ψ with mean values shown for each ply combination

5.4 Cyclic hole elongation parameters

As the specimen was loaded cyclically, there was a flat portion of the response, which corresponds to the slotted hole at the location of the fastener elongating as the fastener bears on the plies. The slotted hole elongation value is denoted by *G* in Figure 19(a). The assumption was that *G* is related to the maximum (or minimum for negative cyclic excursions) relative displacement of the excursion, increasing linearly as the relative displacement increases (Figure 19(b)). The slope of this linear relationship is defined as the hole elongation parameter, $m_G = G/\delta$.

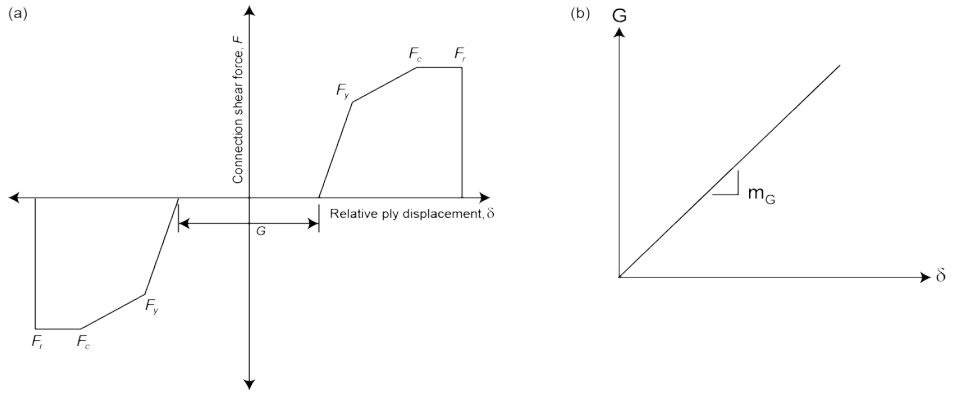

Figure 19: (a) Hole elongation pinching model nomenclature and (b) linear relationship between *G* and relative displacement

To confirm the linear relationship between the relative displacement and *G*, cycles of select sample ply configurations were analyzed to obtain the values for *G*. For each cycle, values for *G*+ and *G*- were extracted, which were defined as the portions of the response with negligible relative change in load and increasing (or decreasing) displacement. The *G*+ value was associated with the maximum relative displacement in the positive excursion, and the *G*- value was associated with the minimum relative displacement in the negative excursion. An example cycle is shown in Figure 20, with the red lines highlighting *G*+ and *G*-.

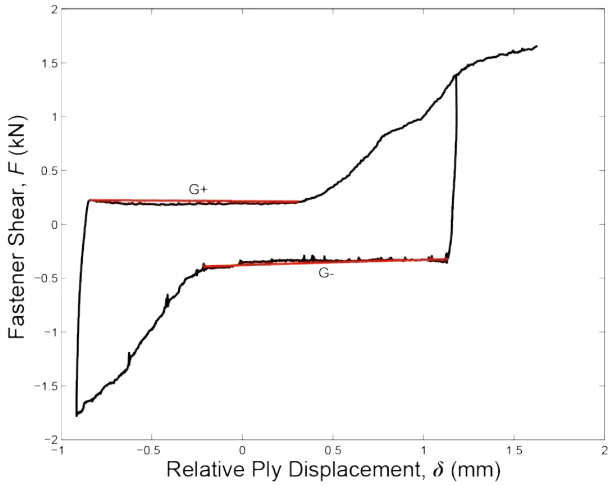

Figure 20: *G*+ and *G*- for cycle 5 of fastener configuration 1854-12-2

A model was developed for the hole elongation parameter, m_G (Figure 21) by fitting a second order polynomial to the data ($m_G = -1.99x10^{-4}\psi^2 + 1.79x10^{-2}\psi + 1.0$).

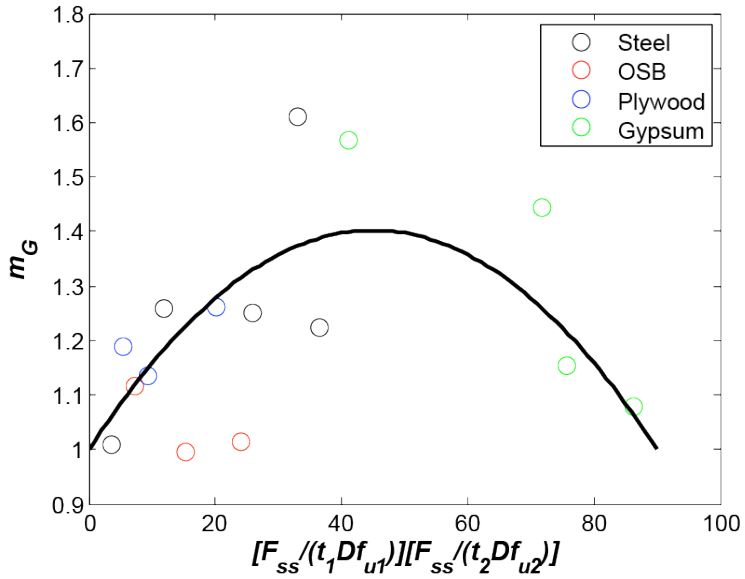

Figure 21: Fastener model for hole elongation parameter, m_G

The hole elongation parameters m_G is related to the pinching parameters as m_G = *rDispP* + *rDispN*, since *rDispP* represents the ratio of reloading displacement in the positive direction to the maximum historic deformation demand, whereas *rDispN* is the same quantity in the negative direction (see Figure 15). The assumed relationship between m_G and ψ is confirmed by plots between *rDispP* + *rDispN* and ψ shown in Figure 22. The fitted polynomial in this case is again a second order polynomial, however the coefficients are different from the trend shown in Figure 21, $rDispP + rDispN = -1x10^{-3}\psi^2 + 8.5x10^{-2}\psi + 0.5$

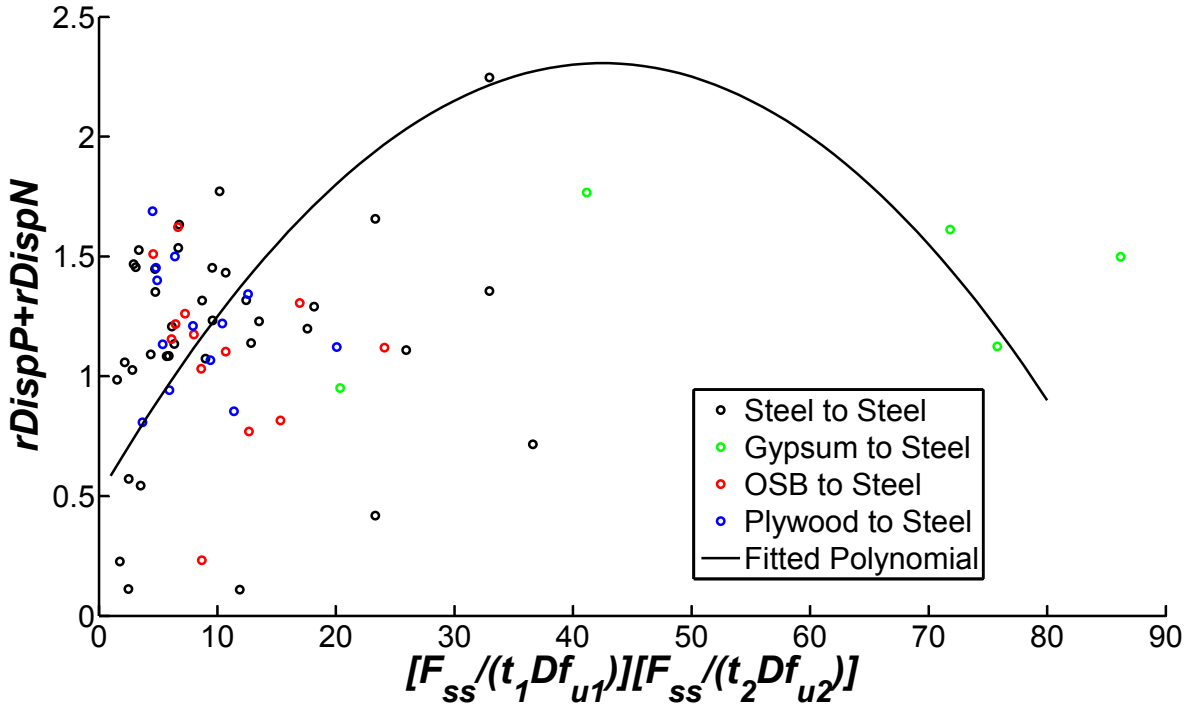

Figure 22 -- Variation in hole elongation parameter obtained from pinching model with ψ

It was found that the connection behavior during the cyclic loading and failure mode affected the amount of hole elongation. The typical failure modes are fastener shear, ply bearing, or fastener tilting and bearing. A smaller ψ typically represents a ply combination with either strong plies (thick or high ultimate stress) or small fasteners. Ply combinations with a smaller ψ were observed to fail predominantly in fastener shear. A larger ψ typically represents a ply combination with either weak plies (thin or low ultimate stress) or large fasteners. These combinations experienced fastener bearing when loaded. With ψ values in between, the properties of the two plies were more related, which resulted in tilting.

The model above shows that there is comparatively less hole elongation at very small and very large ψ. A fastener shear failure (small ψ) indicates that the fastener is the weakest component. More forces transfer into shearing the fastener, which means less forces transfer into ply bearing and consequently, less hole elongation. When tilting occurs at medium ψ, there is more bearing area between the plies and the fastener, which creates more hole elongation. Ply combinations with fastener bearing will have the fastener moving to the prescribed loading protocol, meaning m_G=1 (less hole elongation).

Figure 23(a)-(c) show three ply combinations (small ψ, medium ψ, large ψ, respectively) that were analyzed cycle-by-cycle to obtain G for each cycle to calculate m_G. Each data point is a value for G specific to the cyclic excursion, the green lines represent the fitted line, and the red lines represent m_G=1. Figure 23(a) and (c) show the relationship for ply combinations that experience fastener shear and fastener bearing, respectively. The fitted lines are located nearly or over the red lines. Figure 23(b) shows the relationship for ply combinations that had the fastener tilting on the connection, thus, leading to more hole elongation. It can be seen that the slope of

the fitted lines are much higher than that of the other ply combinations shown, which represents more hole elongation and is consistent with the model.

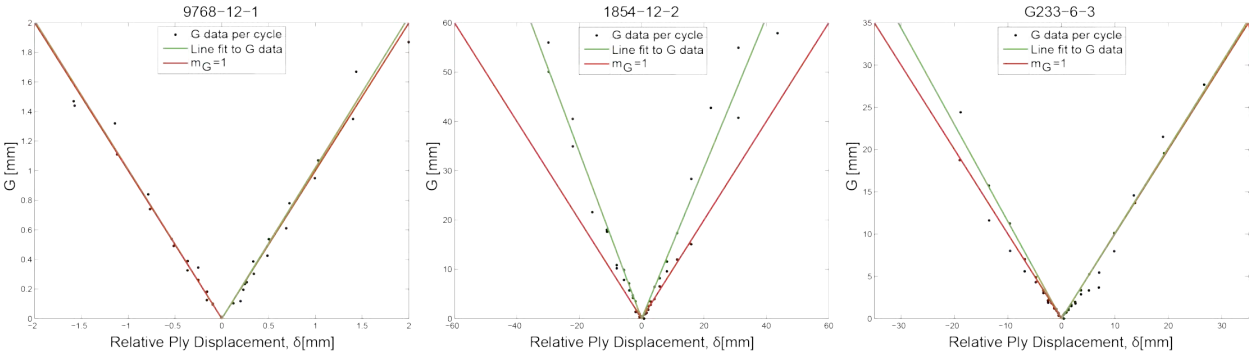

Figure 23: Hole elongation parameter, m_G, plots for (a) small ψ, (b) medium ψ, and (c) large ψ

6 Conclusions

This report makes an important step towards cold-formed steel framed whole building seismic analysis with single shear steel fastener connection backbone, fastener shear failure, pinching, and hole elongation parameter models. The models were derived with data from an extensive experimental program considering monotonic and cyclic loadings, where bearing strengths of the connected plies were the primary parameters influencing pre-peak connection stiffness and strength, hole elongation, and fastener shear. This work also provides updates and improvements to the typical screw fastener connection test setup, defines a means for generalizing cyclic loading protocols for fasteners, and validates a non-contact computer-vision measurement system that conveniently and accurately measures relative displacement throughout the load-deformation response.

Acknowledgements

The authors would like to thank the American Iron and Steel Institute for their financial support and the AISI-facilitated project monitoring task group for their technical support, Simpson Strong-Tie and ELCO Construction Products for donating the fasteners, and ClarkDietrich Building Systems for donating the steel plies. Dr. Matt Eatherton and Dr. David Padilla-Llano made significant contributions that are much appreciated.

References

AISI S905-13 (2013). “Test Standard for Cold-Formed Steel Connections.” American Iron and Steel Institute, Washington, D.C.

AISI S100-12 (2012). “North American Specification for the Design of Cold-Formed Steel Structural Members.” American Iron and Steel Institute, Washington, D.C.

ASTM D5764-97a (2013). “Standard Test Method for Evaluating Dowel-Bearing Strength of Wood and Wood-Based Products.” ASTM International, West Conshohocken, PA.

ASTM E8M-13 (2004). “Standard Test Methods for Tension Testing of Metallic Materials (Metric).” ASTM International, West Conshohocken, PA.

Ayhan, D. and Schafer, B.W. (2016). “The Effect of M/V Ratio on Ledger-Framing Performance of Cold-Formed Steel Buildings.” International Colloquium on Stability and Ductility of Steel Structures – SDSS2016, Timisoara, Romania.

Bian, G., Buonopane, S.G., Ngo, H.H., and Schafer, B.W. (2014). “Fastener-based computational models with application to cold-formed steel shear walls”, 22nd International Specialty Conference on Cold-Formed Steel Structures, St. Louis, MO.

Chatterjee, A., Rogers, C. A. and Moen, C.D. (2017). “High Fidelity Monotonic and Cyclic Simulation of a Wood-sheathed Cold-Formed Steel Framed Floor Diaphragm” 16th World Conference on Earthquake Engineering – WCEE2017, Santiago, Chile

Corner, S. (2014). “Screw-Fastened Cold-Formed Steel-to-Steel Shear Connection Behavior and Models”, M/Sc. thesis, Virginia Tech.

Ding, C. (2015). “Monotonic and Cyclic Simulation of Screw-Fastened Connections for ColdFormed Steel Framing”, M/Sc. thesis, Virginia Tech.

FEMA (2007). “FEMA 461 - Interim protocols for determining seismic performance characteristics of structural and nonstructural components through laboratory testing.” Federal Emergency Management Agency (FEMA), Document No. FEMA 461. Washington, D.C.

FEMA (2009). “FEMA P695 - Quantification of Building Seismic Performance Factors.” Federal Emergency Management Agency (FEMA), Document No. FEMA 965. 2009, Washington, D.C.

Fülöp, L. and Dubina, D. (2006). "Design Criteria for Seam and Sheeting-to-Framing Connections of Cold-Formed Steel Shear Panels." J. Struct. Eng., 132:4, 582-590.

Haus, A. and Moen, C.D. (2014). “Energy Dissipation of Cold-Formed Steel Connections.” Virginia Tech Research Report No. CE/VPI-ST-14/02, Blacksburg, VA.

Ibarra, L.F., Medina, R.A., and Krawinkler, H. (2005). “Hysteretic models that incorporate strength and stiffness deterioration.” Earthquake Engineering & Structural Dynamics, 34(12), 1489-1511.

Lowes, L., Mitra, N., and Altoontash, A. (2004): “A Beam-Column Joint Model for Simulating the Earthquake Response of Reinforced Concrete Frames”. PEER Report 2003/10. Berkeley, CA.

Matlab, Version 8.6.0.267246. The Mathworks, Inc., www.mathworks.com, 2015.

Moen, C.D., Padilla-Llano, D.A., Corner, S., and Ding, C. (2014). “Towards Load-Deformation Models for Screw-Fastened Cold-Formed Steel-to-Steel Shear Connections.” 22nd International Specialty Conference on Cold-Formed Steel Structures, St. Louis, MO.

Moen, C.D., Tao, F., and Cole, R. (2016). “Monotonic and Cyclic Backbone Response of Single Shear Cold-Formed Steel Screw-Fastened Connections.” International Colloquium on Stability and Ductility of Steel Structures – SDSS2016, Timisoara, Romania.

Ngo, H.H. (2014). "Numerical and experimental studies of wood sheathed cold-formed steel framed shear walls”, M.Sc. thesis, Johns Hopkins University.

Niari, S.E., Rafezy, B., and Abedi, K. (2012). “Numerical Modeling and Finite Element Analysis of Steel Sheathed Cold-Formed Steel Shear Walls.” Proceedings of the 15th World Conference on Earthquake Engineering, Lisbon, Portugal.

Okasha, A.F. (2004). “Performance of steel frame/wood sheathing screw connections subjected to monotonic and cyclic loading.” M.Sc. thesis, McGill University.

Padilla-Llano, D.A. (2015). “A Framework for Cyclic Simulation of Thin-Walled Cold-Formed Steel Members in Structural Systems”, PhD dissertation, Virginia Tech.

Pekelnicky, R. and Poland, C. (2012). “ASCE 41-13: Seismic Evaluation and Retrofit of Existing Buildings.” SEAOC 2012 Convention Proceedings, Santa Fe, NM.

Peköz, T. (1990). "Design of cold-formed steel screwed connections." Tenth International Specialty Conference on Cold-formed Steel Structures, Missouri S&T, St. Louis, MO.

Peterman, K., Nakata, N., and Schafer, B.W. (2014). “Hysteretic Characterization of Cold-Formed Steel Stud-to-Sheathing Connections.” Journal of Constructional Steel Research, 101: 254-264.

Peterman, K. and Schafer, B. W. (2013). “Hysteretic shear response of fasteners connecting sheathing to cold-formed steel studs”. CFS NEES: Advancing Cold-Formed Steel Earthquake Engineering

Pham, H. and Moen, C.D. (2015). “Stiffness and Strength of Single Shear Cold-Formed Steel Screw-Fastened Connections”, Virginia Tech Research Report No. CE/VPI-ST-15/07, Blacksburg, VA.

Rogers, C.A. and Hancock, G.J. (1999). “Screwed connection tests of thin G550 and G300 sheet steels”, J. Struct. Eng., 125(2), 128-136.

SFIA, Technical Guide for Cold‐Formed Steel Framing Products, Steel Framing Industry Association, <https://sfia.memberclicks.net/sfia-technical-publications>, February 2, 2016.

Appendix A: Matlab video post-processing code

The following Matlab code can be used to track red targets in a video in .wmv format. The code can be modified to track green or blue targets, and the sensitivity of the tracking to the colors can also be adjusted (redThread, greenThresh, blueThresh). This function outputs a .mat file with the timestamps, centroidal coordinates (x and y) of each recognized target, and the area of each recognized target per frame.

```
function [targetX,targetY,areaTarget,timeCamera] = RGB_VideoOffline(testnumber,camview)

%% Initialization
redThresh = 0.30; % Threshold for red detection
greenThresh = 0.31; % Threshold for green detection
blueThresh = 0.35; % Threshold for blue detection

% vidDevice = imaq.VideoDevice('winvideo', 1, 'YUY2_640x480', ... % Acquire input video stream
%                 'ROI', [1 1 640 480], ...
%                 'ReturnedColorSpace', 'rgb');
% vidInfo = imaqhwinfo(vidDevice); % Acquire input video property
if strcmp(camview,'Angle')==1
   hblob = vision.BlobAnalysis('AreaOutputPort', true, ... % Set blob analysis handling
                               'CentroidOutputPort', true, ...
                               'BoundingBoxOutputPort', true', ...
                               'MinimumBlobArea', 100, ...
                               'MaximumBlobArea', 2500, ...
                               'MaximumCount', 10);
elseif strcmp(camview,'Disp')==1
   hblob = vision.BlobAnalysis('AreaOutputPort', true, ... % Set blob analysis handling
                               'CentroidOutputPort', true, ...
                               'BoundingBoxOutputPort', true', ...
                               'MinimumBlobArea', 1300, ...
                               'MaximumBlobArea', 2000, ...
                               'MaximumCount', 10);
end
hshapeinsBox = vision.ShapeInserter('BorderColorSource', 'Input port', ... % Set box handling
                                    'Fill', true, ...
                                    'FillColorSource', 'Input port', ...
                                    'Opacity', 0.4);
htextinsRed = vision.TextInserter('Text', 'Red   : %2d', ... % Set text for number of blobs
                               'Location',  [5 2], ...
                               'Color', [1 0 0], ... // red color
                               'Font', 'Courier New', ...
                               'FontSize', 14);
htextinsGreen = vision.TextInserter('Text', 'Green : %2d', ... % Set text for number of blobs
                               'Location',  [5 18], ...
                               'Color', [0 1 0], ... // green color
                               'Font', 'Courier New', ...
                               'FontSize', 14);
htextinsBlue = vision.TextInserter('Text', 'Blue  : %.2f', ... % Set text for number of blobs
                               'Location',  [5 34], ...
                               'Color', [0 0 1], ... // blue color
                               'Font', 'Courier New', ...
```

```
                        'FontSize', 14);
htextinsCent = vision.TextInserter('Text', '+      X:%.2f,Y:%.2f', ... % set text for centroid
                        'LocationSource', 'Input port', ...
                        'Color', [0 0 0], ... // yellow color
                        'Font', 'Arial', ...
                        'FontSize', 14);
hVideoOut = vision.VideoPlayer('Name', 'Final Video', ... % Output video player
                    'Position', [100 100 640 480]);
nFrame = 1; % Frame number initialization

%% Processing Loop
vidname=[testnumber,'-',camview];
vidDevice=VideoReader([vidname,'.wmv']); % Read video file
FrameTime=vidDevice.Duration/vidDevice.NumberofFrames;

for nFrame = 1:(vidDevice.NumberOfFrames)
   rgbFrame=vidDevice.read(nFrame);
   %rgbFrame = flipdim(rgbFrame,2); % obtain the mirror image for displaying

   diffFrameRed = imsubtract(rgbFrame(:,:,1), rgb2gray(rgbFrame)); % Get red component of the image
   binFrameRed = im2bw(diffFrameRed, redThresh); % Convert the image into binary image with the red objects as
white

   [areaRed centroidRed, bboxRed] = step(hblob, binFrameRed); % Get the centroids and bounding boxes of the red
blobs
   centroidRed = double(centroidRed); % Convert the centroids into Integer for further steps
   areaRed = double(areaRed);
   vidIn = step(hshapeinsBox, rgbFrame, bboxRed, uint8([1 0 0])); % Insert the red box
   for object = 1:1:length(bboxRed(:,1)) % Write the corresponding centroids for red
      centXRedD = centroidRed(object,1); centYRedD = centroidRed(object,2);
      vidIn = step(htextinsCent, vidIn, [centXRedD centYRedD], [uint16(centXRedD-6) uint16(centYRedD-9)]);
      step(hVideoOut, vidIn)

      centXRed(object,:) = centroidRed(object,1);
      centYRed(object,:) = centroidRed(object,2);
      areaRed(object,:) = areaRed(object,1);

      targetX(object,nFrame) = centXRed(object,:);
      targetY(object,nFrame) = centYRed(object,:);
      areaTarget(object,nFrame) = areaRed(object,1);
   end
   timeCamera(nFrame,:) = (nFrame-1)*FrameTime;
end

targetX = targetX';
targetY = targetY';
areaTarget = areaTarget';
timeCamera = timeCamera-timeCamera(1);

if exist([camview,'RawCamera.mat'],'file')
   delete([camview,'RawCamera.mat'])
end
save([camview,'RawCamera.mat'],'targetX','targetY','areaTarget','timeCamera');

%% Clearing Memory
release(hVideoOut);
```

Appendix B: Steel material tests results

The following figures show the stress-strain curves of all steel plies. Three tensile coupon tests were run for each ply, with the exception of the 97-mil ply from the first batch of the steel (Figure B1(f)). The displacement recordings from the extensometer were inaccurate before yield during the third trial of the 97-mil ply, and the trial was subsequently discarded. Figure B1(a)-(f) show the first batch of steel, and Figure B2(a)-(e) show the second batch of steel.

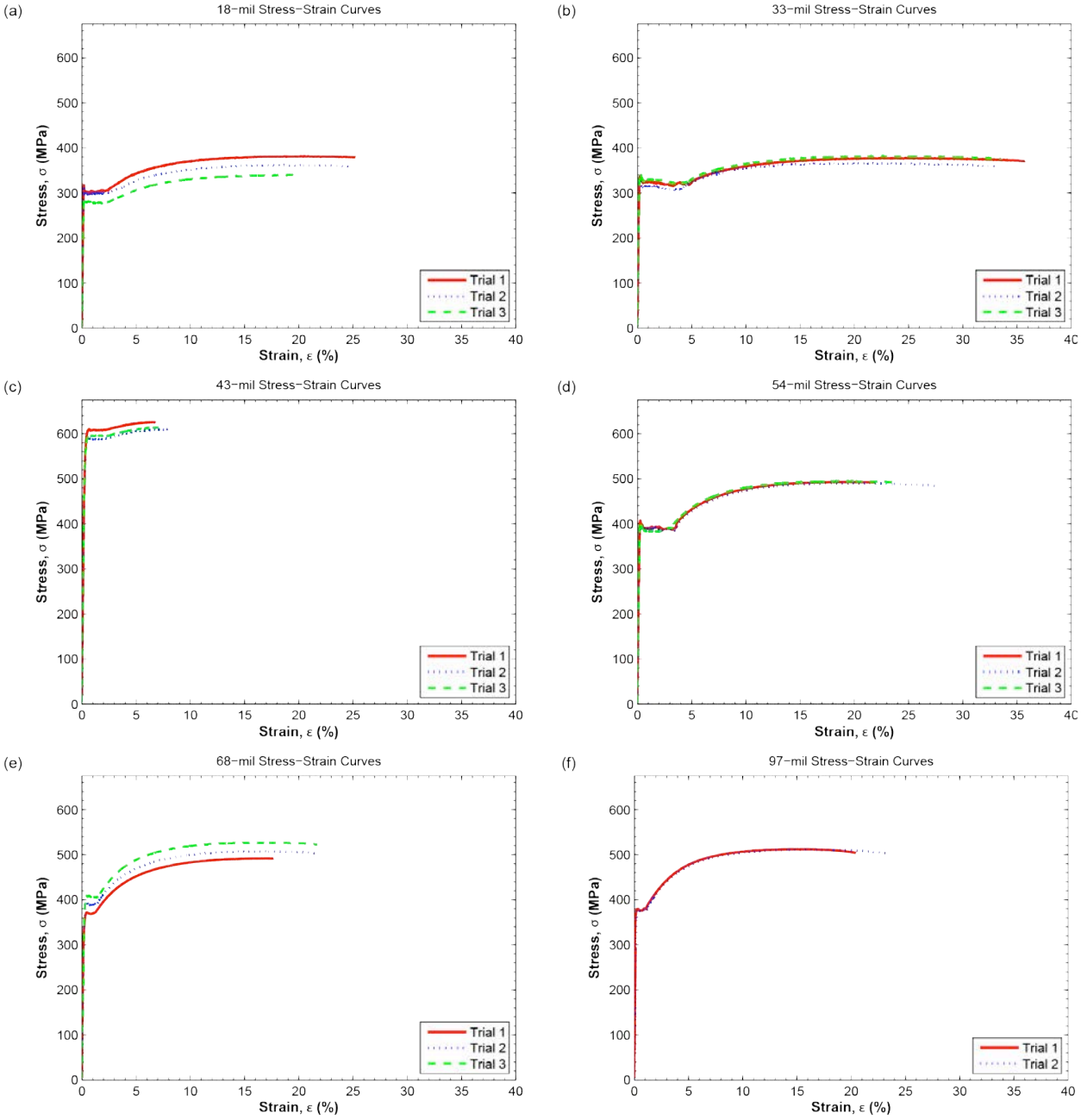

Figure B1: Steel stress-strain curves for Delivery 1; (a) 18-mil, (b) 33-mil, (c) 43-mil, (d) 54-mil, (e) 68-mil, (f) 97-mil

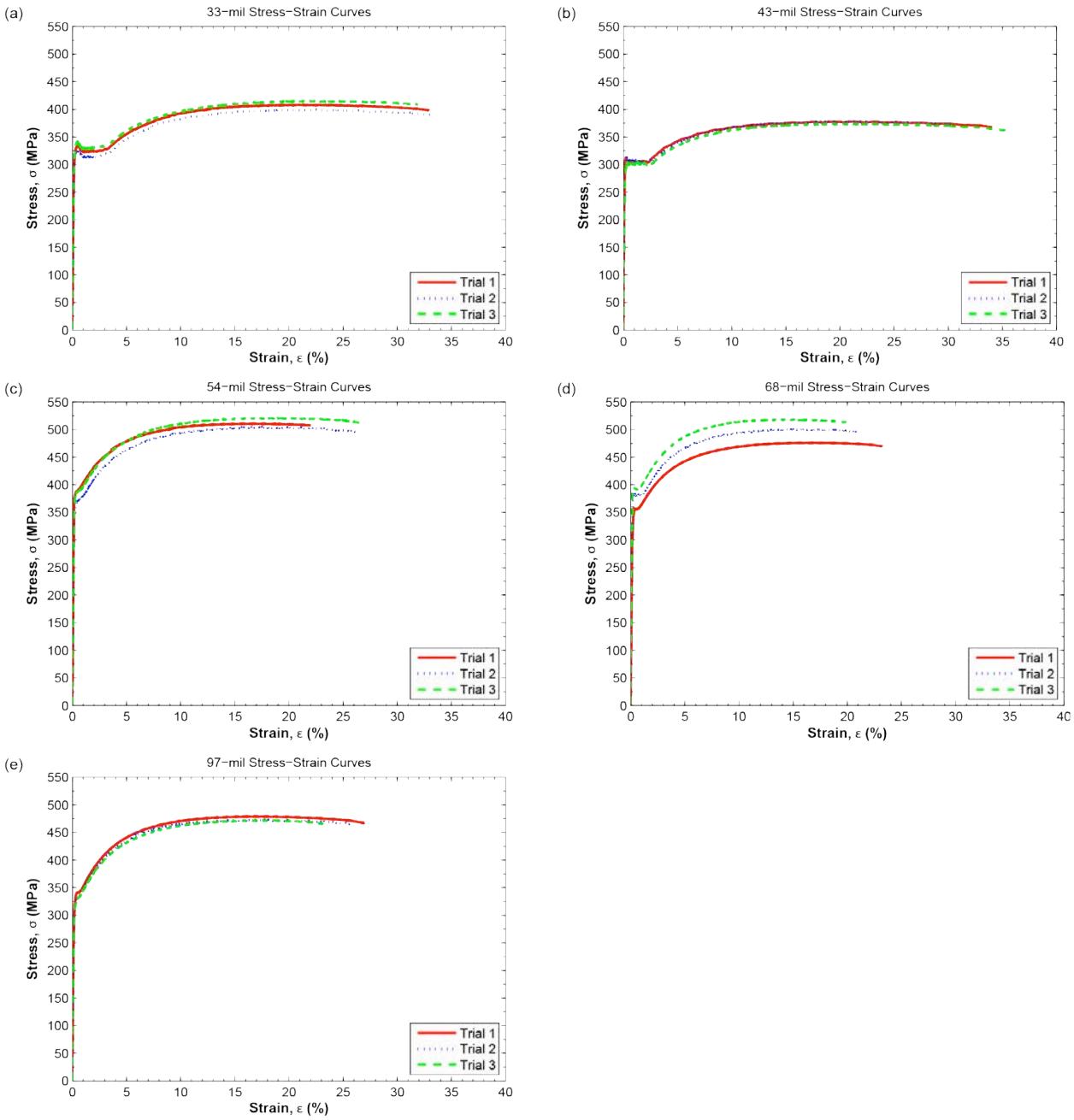

Figure B2: Steel stress-strain curves for Delivery 2; (a) 33-mil, (b) 43-mil, (c) 54-mil, (d) 68-mil, (e) 97-mil

Table B1: Ply parameters for each monotonic experiment

Combination	Steel	t_1 *(mm)*	t_2 [mm]	f_{u1} [Mpa]	f_{u2} [MPa]	D [mm]	F_{ss} [kN]	ψ
2654-08-M1	old	0.50	1.43	361	493	4.20	4.9	10.70
2654-08-M2	old	0.50	1.43	361	493	4.20	4.9	10.70
2654-08-M3	old	0.50	1.43	361	493	4.20	4.9	10.70
2654-10-M1	old	0.50	1.43	361	493	4.74	8.2	23.32
2654-10-M2	old	0.50	1.43	361	493	4.74	8.2	23.32
2654-10-M3	old	0.50	1.43	361	493	4.74	8.2	23.32
2654-12-M1	new	0.50	1.44	361	512	5.40	11.1	31.39
2654-12-M2	old	0.50	1.43	361	493	5.40	11.1	32.96
2654-12-M3	old	0.50	1.43	361	493	5.40	11.1	32.96
3333-08-M1	old	0.90	0.90	376	376	4.20	4.9	11.89
3333-08-M2	old	0.90	0.90	376	376	4.20	4.9	11.89
3333-08-M3	old	0.90	0.90	376	376	4.20	4.9	11.89
3333-10-M1	old	0.90	0.90	376	376	4.74	8.2	25.92
3333-10-M2	old	0.90	0.90	376	376	4.74	8.2	25.92
3333-10-M3	old	0.90	0.90	376	376	4.74	8.2	25.92
3333-12-M1	old	0.90	0.90	376	376	5.40	11.1	36.62
3333-12-M2	old	0.90	0.90	376	376	5.40	11.1	36.62
3333-12-M3	old	0.90	0.90	376	376	5.40	11.1	36.62
4333-08-M1	old	1.11	0.90	615	376	4.20	4.9	5.89
4333-08-M2	old	1.11	0.90	615	376	4.20	4.9	5.89
4333-08-M3	old	1.11	0.90	615	376	4.20	4.9	5.89
4333-10-M1	old	1.11	0.90	615	376	4.74	8.2	12.85
4333-10-M2	old	1.11	0.90	615	376	4.74	8.2	12.85
4333-10-M3	old	1.11	0.90	615	376	4.74	8.2	12.85
4333-12-M1	old	1.11	0.90	615	376	5.40	11.1	18.15
4333-12-M2	old	1.11	0.90	615	376	5.40	11.1	18.15
4333-12-M3	old	1.11	0.90	615	376	5.40	11.1	18.15
4343-08-M1	old	1.11	1.11	615	615	4.20	4.9	2.92
4343-08-M2	old	1.11	1.11	615	615	4.20	4.9	2.92
4343-08-M3	old	1.11	1.11	615	615	4.20	4.9	2.92
4343-10-M1	old	1.11	1.11	615	615	4.74	8.2	6.37
4343-10-M2	old	1.11	1.11	615	615	4.74	8.2	6.37
4343-10-M3	old	1.11	1.11	615	615	4.74	8.2	6.37
4343-12-M1	old	1.11	1.11	615	615	5.40	11.1	9.00
4343-12-M2	old	1.11	1.11	615	615	5.40	11.1	9.00
4343-12-M3	old	1.11	1.11	615	615	5.40	11.1	9.00
4354-08-M1	old	1.11	1.43	615	493	4.20	4.9	2.83
4354-08-M2	old	1.11	1.43	615	493	4.20	4.9	2.83
4354-08-M3	old	1.11	1.43	615	493	4.20	4.9	2.83

4354-10-M1	old	1.11	1.43	615	493	4.74	8.2	6.17
4354-10-M2	old	1.11	1.43	615	493	4.74	8.2	6.17
4354-10-M3	old	1.11	1.43	615	493	4.74	8.2	6.17
4354-12-M1	old	1.11	1.43	615	493	5.40	11.1	8.71
4354-12-M2	old	1.11	1.43	615	493	5.40	11.1	8.71
4354-12-M3	old	1.11	1.43	615	493	5.40	11.1	8.71
4368-08-M1	old	1.11	1.80	615	510	4.20	4.9	2.17
4368-08-M2	old	1.11	1.80	615	510	4.20	4.9	2.17
4368-08-M3	old	1.11	1.80	615	510	4.20	4.9	2.17
4368-10-M1	old	1.11	1.80	615	510	4.74	8.2	4.74
4368-10-M2	old	1.11	1.80	615	510	4.74	8.2	4.74
4368-10-M3	old	1.11	1.80	615	510	4.74	8.2	4.74
4368-12-M1	old	1.11	1.80	615	510	5.40	11.1	6.69
4368-12-M2	old	1.11	1.80	615	510	5.40	11.1	6.69
4368-12-M3	old	1.11	1.80	615	510	5.40	11.1	6.69
4397-08-M1	old	1.11	2.56	615	505	4.20	4.9	1.54
4397-08-M2	old	1.11	2.56	615	505	4.20	4.9	1.54
4397-08-M3	old	1.11	2.56	615	505	4.20	4.9	1.54
4397-10-M1	old	1.11	2.56	615	505	4.74	8.2	3.36
4397-10-M2	old	1.11	2.56	615	505	4.74	8.2	3.36
4397-10-M3	old	1.11	2.56	615	505	4.74	8.2	3.36
4397-12-M1	old	1.11	2.56	615	505	5.40	11.1	4.75
4397-12-M2	old	1.11	2.56	615	505	5.40	11.1	4.75
4397-12-M3	old	1.11	2.56	615	505	5.40	11.1	4.75
5426-08-M1	old	1.43	0.50	493	361	4.20	4.9	10.70
5426-08-M2	old	1.43	0.50	493	361	4.20	4.9	10.70
5426-08-M3	old	1.43	0.50	493	361	4.20	4.9	10.70
5426-10-M1	old	1.43	0.50	493	361	4.74	8.2	23.32
5426-10-M2	old	1.43	0.50	493	361	4.74	8.2	23.32
5426-10-M3	old	1.43	0.50	493	361	4.74	8.2	23.32
5426-12-M1	old	1.43	0.50	493	361	5.40	11.1	32.96
5426-12-M2	old	1.43	0.50	493	361	5.40	11.1	32.96
5426-12-M3	old	1.43	0.50	493	361	5.40	11.1	32.96
5433-08-M1	old	1.43	0.90	493	376	4.20	4.9	5.71
5433-08-M2	old	1.43	0.90	493	376	4.20	4.9	5.71
5433-08-M3	old	1.43	0.90	493	376	4.20	4.9	5.71
5433-10-M1	old	1.43	0.90	493	376	4.74	8.2	12.44
5433-10-M2	old	1.43	0.90	493	376	4.74	8.2	12.44
5433-10-M3	old	1.43	0.90	493	376	4.74	8.2	12.44
5433-12-M1	old	1.43	0.90	493	376	5.40	11.1	17.58
5433-12-M2	old	1.43	0.90	493	376	5.40	11.1	17.58
5433-12-M3	old	1.43	0.90	493	376	5.40	11.1	17.58

6833-08-M1	old	1.80	0.90	510	376	4.20	4.9	4.38
6833-08-M2	old	1.80	0.90	510	376	4.20	4.9	4.38
6833-08-M3	old	1.80	0.90	510	376	4.20	4.9	4.38
6833-10-M1	old	1.80	0.90	510	376	4.74	8.2	9.55
6833-10-M2	old	1.80	0.90	510	376	4.74	8.2	9.55
6833-10-M3	old	1.80	0.90	510	376	4.74	8.2	9.55
6833-12-M1	old	1.80	0.90	510	376	5.40	11.1	13.50
6833-12-M2	old	1.80	0.90	510	376	5.40	11.1	13.50
6833-12-M3	old	1.80	0.90	510	376	5.40	11.1	13.50
9733-08-M1	old	2.56	0.90	505	376	4.20	4.9	3.11
9733-08-M2	old	2.56	0.90	505	376	4.20	4.9	3.11
9733-08-M3	old	2.56	0.90	505	376	4.20	4.9	3.11
9733-10-M1	old	2.56	0.90	505	376	4.74	8.2	6.78
9733-10-M2	old	2.56	0.90	505	376	4.74	8.2	6.78
9733-10-M3	old	2.56	0.90	505	376	4.74	8.2	6.78
9733-12-M1	old	2.56	0.90	505	376	5.40	11.1	9.59
9733-12-M2	old	2.56	0.90	505	376	5.40	11.1	9.59
9733-12-M3	old	2.56	0.90	505	376	5.40	11.1	9.59
9768-10-M1	old	2.56	1.80	505	510	4.74	8.2	2.50
9768-10-M2	old	2.56	1.80	505	510	4.74	8.2	2.50
9768-10-M3	old	2.56	1.80	505	510	4.74	8.2	2.50
9768-12-M1	old	2.56	1.80	505	510	5.40	11.1	3.53
9768-12-M2	old	2.56	1.80	505	510	5.40	11.1	3.53
9768-12-M3	old	2.56	1.80	505	510	5.40	11.1	3.53
9797-10-M1	old	2.56	2.56	505	505	4.74	8.2	1.78
9797-10-M2	old	2.56	2.56	505	505	4.74	8.2	1.78
9797-10-M3	old	2.56	2.56	505	505	4.74	8.2	1.78
9797-12-M1	old	2.56	2.56	505	505	5.40	11.1	2.51
9797-12-M2	old	2.56	2.56	505	505	5.40	11.1	2.51
9797-12-M3	old	2.56	2.56	505	505	5.40	11.1	2.51
G133-06-M1	new	9.6	0.86	10.3	408	3.45	5.6	75.80
G133-06-M2	new	9.6	0.86	10.3	408	3.45	5.6	75.80
G133-06-M3	new	9.6	0.86	10.3	408	3.45	5.6	75.80
G233-6-M1	new	12.573	0.86	6.88	408	3.45	5.6	86.19
G233-6-M2	new	12.573	0.86	6.88	408	3.45	5.6	86.19
G233-6-M3	new	12.573	0.86	6.88	408	3.45	5.6	86.19
G243-6-M1	old	12.573	1.11	6.88	615	3.45	5.6	44.62
G243-6-M2	old	12.573	1.11	6.88	615	3.45	5.6	44.62
G243-6-M3	old	12.573	1.11	6.88	615	3.45	5.6	44.62
G254-6-M1	new	12.573	1.44	6.88	512	3.45	5.6	41.15
G254-6-M2	new	12.573	1.44	6.88	512	3.45	5.6	41.15
G254-6-M3	new	12.573	1.44	6.88	512	3.45	5.6	41.15

G354-06-M1	new	16.1	1.44	10.9	512	3.45	5.6	20.34
G354-06-M2	new	16.1	1.44	10.9	512	3.45	5.6	20.34
G354-06-M3	new	16.1	1.44	10.9	512	3.45	5.6	20.34
O133-08-M1	old	11.6	0.90	33.4	376	4.14	7.5	24.96
O133-08-M2	old	11.6	0.90	33.4	376	4.14	7.5	24.96
O133-08-M3	old	11.6	0.90	33.4	376	4.14	7.5	24.96
O233-08-M1	old	14.9	0.90	40.9	376	4.14	7.5	15.88
O233-08-M2	old	14.9	0.90	40.9	376	4.14	7.5	15.88
O233-08-M3	old	14.9	0.90	40.9	376	4.14	7.5	15.88
O233-10-M1	old	14.9	0.90	40.9	376	4.67	8.9	17.54
O233-10-M2	new	14.9	0.86	40.9	408	4.67	8.9	16.93
O233-10-M3	new	14.9	0.86	40.9	408	4.67	8.9	16.93
O243-08-M1	old	14.9	1.11	40.9	615	4.14	7.5	7.87
O243-08-M2	old	14.9	1.11	40.9	615	4.14	7.5	7.87
O243-08-M3	old	14.9	1.11	40.9	615	4.14	7.5	7.87
O243-10-M1	old	14.9	1.11	40.9	615	4.67	8.9	8.70
O243-10-M2	old	14.9	1.11	40.9	615	4.67	8.9	8.70
O243-10-M3	old	14.9	1.11	40.9	615	4.67	8.9	8.70
O254-08-M1	new	14.9	1.44	40.9	512	4.14	7.5	7.26
O254-08-M2	new	14.9	1.44	40.9	512	4.14	7.5	7.26
O254-08-M3	new	14.9	1.44	40.9	512	4.14	7.5	7.26
O254-10-M1	new	14.9	1.44	40.9	512	4.67	8.9	8.02
O254-10-M2	new	14.9	1.44	40.9	512	4.67	8.9	8.02
O254-10-M3	new	14.9	1.44	40.9	512	4.67	8.9	8.02
O254-12-M1	new	14.9	1.44	40.9	512	5.41	11.9	10.70
O254-12-M2	new	14.9	1.44	40.9	512	5.41	11.9	10.70
O254-12-M3	new	14.9	1.44	40.9	512	5.41	11.9	10.70
O268-10-M1	old	14.9	1.80	40.9	510	4.67	8.9	6.47
O268-10-M2	old	14.9	1.80	40.9	510	4.67	8.9	6.47
O268-10-M3	old	14.9	1.80	40.9	510	4.67	8.9	6.47
O268-12-M1	old	14.9	1.80	40.9	510	5.41	11.9	8.63
O268-12-M2	old	14.9	1.80	40.9	510	5.41	11.9	8.63
O268-12-M3	old	14.9	1.80	40.9	510	5.41	11.9	8.63
O297-10-M1	old	14.9	2.56	40.9	505	4.67	8.9	4.59
O297-10-M2	old	14.9	2.56	40.9	505	4.67	8.9	4.59
O297-10-M3	old	14.9	2.56	40.9	505	4.67	8.9	4.59
O297-12-M1	old	14.9	2.56	40.9	505	5.41	11.9	6.13
O297-12-M2	old	14.9	2.56	40.9	505	5.41	11.9	6.13
O297-12-M3	old	14.9	2.56	40.9	505	5.41	11.9	6.13
O397-12-M1	new	17.9	2.52	33.8	475	5.41	11.9	6.68
O397-12-M2	new	17.9	2.52	33.8	475	5.41	11.9	6.68
O397-12-M3	new	17.9	2.52	33.8	475	5.41	11.9	6.68

P133-08-M1	new	11.4	0.86	41	408	4.14	7.5	20.06
P133-08-M2	new	11.4	0.86	41	408	4.14	7.5	20.06
P133-08-M3	new	11.4	0.86	41	408	4.14	7.5	20.06
P233-08-M1	new	14.7	0.86	56.1	408	4.14	7.5	11.39
P233-08-M2	new	14.7	0.86	56.1	408	4.14	7.5	11.39
P233-08-M3	new	14.7	0.86	56.1	408	4.14	7.5	11.39
P233-10-M1	new	14.7	0.86	56.1	408	4.67	8.9	12.58
P233-10-M2	new	14.7	0.86	56.1	408	4.67	8.9	12.58
P233-10-M3	new	14.7	0.86	56.1	408	4.67	8.9	12.58
P243-08-M1	new	14.7	1.12	56.1	377	4.14	7.5	9.41
P243-08-M2	new	14.7	1.12	56.1	377	4.14	7.5	9.41
P243-08-M3	new	14.7	1.12	56.1	377	4.14	7.5	9.41
P243-10-M1	new	14.7	1.12	56.1	377	4.67	8.9	10.40
P243-10-M2	new	14.7	1.12	56.1	377	4.67	8.9	10.40
P243-10-M3	new	14.7	1.12	56.1	377	4.67	8.9	10.40
P254-08-M1	new	14.7	1.44	56.1	512	4.14	7.5	5.39
P254-08-M2	new	14.7	1.44	56.1	512	4.14	7.5	5.39
P254-08-M3	new	14.7	1.44	56.1	512	4.14	7.5	5.39
P254-10-M1	new	14.7	1.44	56.1	512	4.67	8.9	5.96
P254-10-M2	new	14.7	1.44	56.1	512	4.67	8.9	5.96
P254-10-M3	new	14.7	1.44	56.1	512	4.67	8.9	5.96
P254-12-M1	new	14.7	1.44	56.1	512	5.41	11.9	7.95
P254-12-M2	new	14.7	1.44	56.1	512	5.41	11.9	7.95
P254-12-M3	new	14.7	1.44	56.1	512	5.41	11.9	7.95
P268-10-M1	old	14.7	1.80	56.1	510	4.67	8.9	4.80
P268-10-M2	old	14.7	1.80	56.1	510	4.67	8.9	4.80
P268-10-M3	old	14.7	1.80	56.1	510	4.67	8.9	4.80
P268-12-M1	old	14.7	1.80	56.1	510	5.41	11.9	6.41
P268-12-M2	old	14.7	1.80	56.1	510	5.41	11.9	6.41
P268-12-M3	old	14.7	1.80	56.1	510	5.41	11.9	6.41
P297-10-M1	new	14.7	2.52	56.1	475	4.67	8.9	3.68
P297-10-M2	new	14.7	2.52	56.1	475	4.67	8.9	3.68
P297-10-M3	new	14.7	2.52	56.1	475	4.67	8.9	3.68
P297-12-M1	new	14.7	2.52	56.1	475	5.41	11.9	4.92
P297-12-M2	new	14.7	2.52	56.1	475	5.41	11.9	4.92
P297-12-M3	new	14.7	2.52	56.1	475	5.41	11.9	4.92
P397-12-M1	new	17.3	2.52	51.4	475	5.41	11.9	4.54
P397-12-M2	new	17.3	2.52	51.4	475	5.41	11.9	4.54
P397-12-M3	new	17.3	2.52	51.4	475	5.41	11.9	4.54

Table B2: Ply parameters for each cyclic experiment

Combination	Steel	t_1 *(mm)*	t_2 [mm]	f_{u1} [Mpa]	f_{u2} [MPa]	D [mm]	F_{ss} [kN]	ψ
2654-08-C1	new	0.50	1.44	361	512	4.20	4.9	10.19
2654-08-C2	new	0.50	1.44	361	512	4.20	4.9	10.19
2654-08-C3	old	0.50	1.43	361	493	4.20	4.9	10.70
2654-10-C1	old	0.50	1.43	361	493	4.74	8.2	23.32
2654-10-C2	old	0.50	1.43	361	493	4.74	8.2	23.32
2654-10-C3	old	0.50	1.43	361	493	4.74	8.2	23.32
2654-12-C1	old	0.50	1.43	361	493	5.40	11.1	32.96
2654-12-C2	old	0.50	1.43	361	493	5.40	11.1	32.96
2654-12-C3	new	0.50	1.44	361	512	5.40	11.1	31.39
3333-08-C1	old	0.90	0.90	376	376	4.20	4.9	11.89
3333-08-C2	old	0.90	0.90	376	376	4.20	4.9	11.89
3333-08-C3	old	0.90	0.90	376	376	4.20	4.9	11.89
3333-10-C1	old	0.90	0.90	376	376	4.74	8.2	25.92
3333-10-C2	old	0.90	0.90	376	376	4.74	8.2	25.92
3333-10-C3	old	0.90	0.90	376	376	4.74	8.2	25.92
3333-12-C1	old	0.90	0.90	376	376	5.40	11.1	36.62
3333-12-C2	old	0.90	0.90	376	376	5.40	11.1	36.62
3333-12-C3	old	0.90	0.90	376	376	5.40	11.1	36.62
4333-08-C1	old	1.11	0.90	615	376	4.20	4.9	5.89
4333-08-C2	old	1.11	0.90	615	376	4.20	4.9	5.89
4333-08-C3	old	1.11	0.90	615	376	4.20	4.9	5.89
4333-10-C1	old	1.11	0.90	615	376	4.74	8.2	12.85
4333-10-C2	old	1.11	0.90	615	376	4.74	8.2	12.85
4333-10-C3	old	1.11	0.90	615	376	4.74	8.2	12.85
4333-12-C1	old	1.11	0.90	615	376	5.40	11.1	18.15
4333-12-C2	old	1.11	0.90	615	376	5.40	11.1	18.15
4333-12-C3	old	1.11	0.90	615	376	5.40	11.1	18.15
4343-08-C1	old	1.11	1.11	615	615	4.20	4.9	2.92
4343-08-C2	old	1.11	1.11	615	615	4.20	4.9	2.92
4343-08-C3	old	1.11	1.11	615	615	4.20	4.9	2.92
4343-10-C1	old	1.11	1.11	615	615	4.74	8.2	6.37
4343-10-C2	old	1.11	1.11	615	615	4.74	8.2	6.37
4343-10-C3	old	1.11	1.11	615	615	4.74	8.2	6.37
4343-12-C1	old	1.11	1.11	615	615	5.40	11.1	9.00
4343-12-C2	old	1.11	1.11	615	615	5.40	11.1	9.00
4343-12-C3	old	1.11	1.11	615	615	5.40	11.1	9.00
4354-08-C1	old	1.11	1.43	615	493	4.20	4.9	2.83
4354-08-C2	old	1.11	1.43	615	493	4.20	4.9	2.83
4354-08-C3	old	1.11	1.43	615	493	4.20	4.9	2.83

4354-10-C1	old	1.11	1.43	615	493	4.74	8.2	6.17
4354-10-C2	old	1.11	1.43	615	493	4.74	8.2	6.17
4354-10-C3	old	1.11	1.43	615	493	4.74	8.2	6.17
4354-12-C1	old	1.11	1.43	615	493	5.40	11.1	8.71
4354-12-C2	old	1.11	1.43	615	493	5.40	11.1	8.71
4354-12-C3	old	1.11	1.43	615	493	5.40	11.1	8.71
4368-08-C1	old	1.11	1.80	615	510	4.20	4.9	2.17
4368-08-C2	old	1.11	1.80	615	510	4.20	4.9	2.17
4368-08-C3	old	1.11	1.80	615	510	4.20	4.9	2.17
4368-10-C1	old	1.11	1.80	615	510	4.74	8.2	4.74
4368-10-C2	old	1.11	1.80	615	510	4.74	8.2	4.74
4368-10-C3	old	1.11	1.80	615	510	4.74	8.2	4.74
4368-12-C1	old	1.11	1.80	615	510	5.40	11.1	6.69
4368-12-C2	old	1.11	1.80	615	510	5.40	11.1	6.69
4368-12-C3	old	1.11	1.80	615	510	5.40	11.1	6.69
4397-08-C1	old	1.11	2.56	615	505	4.20	4.9	1.54
4397-08-C2	old	1.11	2.56	615	505	4.20	4.9	1.54
4397-08-C3	old	1.11	2.56	615	505	4.20	4.9	1.54
4397-10-C1	old	1.11	2.56	615	505	4.74	8.2	3.36
4397-10-C2	old	1.11	2.56	615	505	4.74	8.2	3.36
4397-10-C3	old	1.11	2.56	615	505	4.74	8.2	3.36
4397-12-C1	old	1.11	2.56	615	505	5.40	11.1	4.75
4397-12-C2	old	1.11	2.56	615	505	5.40	11.1	4.75
4397-12-C3	old	1.11	2.56	615	505	5.40	11.1	4.75
5426-08-C1	old	1.43	0.50	493	361	4.20	4.9	10.70
5426-08-C2	old	1.43	0.50	493	361	4.20	4.9	10.70
5426-08-C3	old	1.43	0.50	493	361	4.20	4.9	10.70
5426-10-C1	old	1.43	0.50	493	361	4.74	8.2	23.32
5426-10-C2	old	1.43	0.50	493	361	4.74	8.2	23.32
5426-10-C3	old	1.43	0.50	493	361	4.74	8.2	23.32
5426-12-C1	old	1.43	0.50	493	361	5.40	11.1	32.96
5426-12-C2	old	1.43	0.50	493	361	5.40	11.1	32.96
5426-12-C3	old	1.43	0.50	493	361	5.40	11.1	32.96
5433-08-C1	old	1.43	0.90	493	376	4.20	4.9	5.71
5433-08-C2	old	1.43	0.90	493	376	4.20	4.9	5.71
5433-08-C3	old	1.43	0.90	493	376	4.20	4.9	5.71
5433-10-C1	old	1.43	0.90	493	376	4.74	8.2	12.44
5433-10-C2	old	1.43	0.90	493	376	4.74	8.2	12.44
5433-10-C3	old	1.43	0.90	493	376	4.74	8.2	12.44
5433-12-C1	old	1.43	0.90	493	376	5.40	11.1	17.58
5433-12-C2	old	1.43	0.90	493	376	5.40	11.1	17.58
5433-12-C3	old	1.43	0.90	493	376	5.40	11.1	17.58

6833-08-C1	old	1.80	0.90	510	376	4.20	4.9	4.38
6833-08-C2	old	1.80	0.90	510	376	4.20	4.9	4.38
6833-08-C3	old	1.80	0.90	510	376	4.20	4.9	4.38
6833-10-C1	old	1.80	0.90	510	376	4.74	8.2	9.55
6833-10-C2	old	1.80	0.90	510	376	4.74	8.2	9.55
6833-10-C3	old	1.80	0.90	510	376	4.74	8.2	9.55
6833-12-C1	old	1.80	0.90	510	376	5.40	11.1	13.50
6833-12-C2	old	1.80	0.90	510	376	5.40	11.1	13.50
6833-12-C3	old	1.80	0.90	510	376	5.40	11.1	13.50
9733-08-C1	old	2.56	0.90	505	376	4.20	4.9	3.11
9733-08-C2	old	2.56	0.90	505	376	4.20	4.9	3.11
9733-08-C3	old	2.56	0.90	505	376	4.20	4.9	3.11
9733-10-C1	old	2.56	0.90	505	376	4.74	8.2	6.78
9733-10-C2	old	2.56	0.90	505	376	4.74	8.2	6.78
9733-10-C3	old	2.56	0.90	505	376	4.74	8.2	6.78
9733-12-C1	old	2.56	0.90	505	376	5.40	11.1	9.59
9733-12-C2	old	2.56	0.90	505	376	5.40	11.1	9.59
9733-12-C3	old	2.56	0.90	505	376	5.40	11.1	9.59
9768-10-C1	old	2.56	1.80	505	510	4.74	8.2	2.50
9768-10-C2	old	2.56	1.80	505	510	4.74	8.2	2.50
9768-10-C3	old	2.56	1.80	505	510	4.74	8.2	2.50
9768-12-C1	old	2.56	1.80	505	510	5.40	11.1	3.53
9768-12-C2	old	2.56	1.80	505	510	5.40	11.1	3.53
9768-12-C3	old	2.56	1.80	505	510	5.40	11.1	3.53
9797-10-C1	old	2.56	2.56	505	505	4.74	8.2	1.78
9797-10-C2	old	2.56	2.56	505	505	4.74	8.2	1.78
9797-10-C3	old	2.56	2.56	505	505	4.74	8.2	1.78
9797-12-C1	old	2.56	2.56	505	505	5.40	11.1	2.51
9797-12-C2	old	2.56	2.56	505	505	5.40	11.1	2.51
9797-12-C3	old	2.56	2.56	505	505	5.40	11.1	2.51
G133-06-C1	new	9.6	0.86	10.3	408	3.45	5.6	75.80
G133-06-C2	new	9.6	0.86	10.3	408	3.45	5.6	75.80
G133-06-C3	new	9.6	0.86	10.3	408	3.45	5.6	75.80
G233-6-C1	new	12.573	0.86	6.88	408	3.45	5.6	86.19
G233-6-C2	new	12.573	0.86	6.88	408	3.45	5.6	86.19
G233-6-C3	new	12.573	0.86	6.88	408	3.45	5.6	86.19
G243-6-C1	new	12.573	1.12	6.88	377	3.45	5.6	71.83
G243-6-C2	new	12.573	1.12	6.88	377	3.45	5.6	71.83
G243-6-C3	new	12.573	1.12	6.88	377	3.45	5.6	71.83
G254-6-C1	new	12.573	1.44	6.88	512	3.45	5.6	41.15
G254-6-C2	new	12.573	1.44	6.88	512	3.45	5.6	41.15
G254-6-C3	new	12.573	1.44	6.88	512	3.45	5.6	41.15

G354-06-C1	new	16.1	1.44	10.9	512	3.45	5.6	20.34
G354-06-C2	new	16.1	1.44	10.9	512	3.45	5.6	20.34
G354-06-C3	new	16.1	1.44	10.9	512	3.45	5.6	20.34
O133-08-C1	new	11.6	0.86	33.4	408	4.14	7.5	24.09
O133-08-C2	new	11.6	0.86	33.4	408	4.14	7.5	24.09
O133-08-C3	new	11.6	0.86	33.4	408	4.14	7.5	24.09
O233-08-C1	new	14.9	0.86	40.9	408	4.14	7.5	15.32
O233-08-C2	new	14.9	0.86	40.9	408	4.14	7.5	15.32
O233-08-C3	new	14.9	0.86	40.9	408	4.14	7.5	15.32
O233-10-C1	new	14.9	0.86	40.9	408	4.67	8.9	16.93
O233-10-C2	new	14.9	0.86	40.9	408	4.67	8.9	16.93
O233-10-C3	new	14.9	0.86	40.9	408	4.67	8.9	16.93
O243-08-C1	new	14.9	1.12	40.9	377	4.14	7.5	12.67
O243-08-C2	new	14.9	1.12	40.9	377	4.14	7.5	12.67
O243-08-C3	new	14.9	1.12	40.9	377	4.14	7.5	12.67
O243-10-C1	old	14.9	1.11	40.9	615	4.67	8.9	8.70
O243-10-C2	old	14.9	1.11	40.9	615	4.67	8.9	8.70
O243-10-C3	old	14.9	1.11	40.9	615	4.67	8.9	8.70
O254-08-C1	new	14.9	1.44	40.9	512	4.14	7.5	7.26
O254-08-C2	new	14.9	1.44	40.9	512	4.14	7.5	7.26
O254-08-C3	new	14.9	1.44	40.9	512	4.14	7.5	7.26
O254-10-C1	new	14.9	1.44	40.9	512	4.67	8.9	8.02
O254-10-C2	new	14.9	1.44	40.9	512	4.67	8.9	8.02
O254-10-C3	new	14.9	1.44	40.9	512	4.67	8.9	8.02
O254-12-C1	new	14.9	1.44	40.9	512	5.41	11.9	10.70
O254-12-C2	new	14.9	1.44	40.9	512	5.41	11.9	10.70
O254-12-C3	new	14.9	1.44	40.9	512	5.41	11.9	10.70
O268-10-C1	old	14.9	1.80	40.9	510	4.67	8.9	6.47
O268-10-C2	old	14.9	1.80	40.9	510	4.67	8.9	6.47
O268-10-C3	old	14.9	1.80	40.9	510	4.67	8.9	6.47
O268-12-C1	old	14.9	1.80	40.9	510	5.41	11.9	8.63
O268-12-C2	old	14.9	1.80	40.9	510	5.41	11.9	8.63
O268-12-C3	old	14.9	1.80	40.9	510	5.41	11.9	8.63
O297-10-C1	old	14.9	2.56	40.9	505	4.67	8.9	4.59
O297-10-C2	old	14.9	2.56	40.9	505	4.67	8.9	4.59
O297-10-C3	old	14.9	2.56	40.9	505	4.67	8.9	4.59
O297-12-C1	old	14.9	2.56	40.9	505	5.41	11.9	6.13
O297-12-C2	old	14.9	2.56	40.9	505	5.41	11.9	6.13
O297-12-C3	old	14.9	2.56	40.9	505	5.41	11.9	6.13
O397-12-C1	new	17.9	2.52	33.8	475	5.41	11.9	6.68
O397-12-C2	new	17.9	2.52	33.8	475	5.41	11.9	6.68
O397-12-C3	new	17.9	2.52	33.8	475	5.41	11.9	6.68

P133-08-C1	new	11.4	0.86	41	408	4.14	7.5	20.06
P133-08-C2	new	11.4	0.86	41	408	4.14	7.5	20.06
P133-08-C3	new	11.4	0.86	41	408	4.14	7.5	20.06
P233-08-C1	new	14.7	0.86	56.1	408	4.14	7.5	11.39
P233-08-C2	new	14.7	0.86	56.1	408	4.14	7.5	11.39
P233-08-C3	new	14.7	0.86	56.1	408	4.14	7.5	11.39
P233-10-C1	new	14.7	0.86	56.1	408	4.67	8.9	12.58
P233-10-C2	new	14.7	0.86	56.1	408	4.67	8.9	12.58
P233-10-C3	new	14.7	0.86	56.1	408	4.67	8.9	12.58
P243-08-C1	new	14.7	1.12	56.1	377	4.14	7.5	9.41
P243-08-C2	new	14.7	1.12	56.1	377	4.14	7.5	9.41
P243-08-C3	new	14.7	1.12	56.1	377	4.14	7.5	9.41
P243-10-C1	new	14.7	1.12	56.1	377	4.67	8.9	10.40
P243-10-C2	new	14.7	1.12	56.1	377	4.67	8.9	10.40
P243-10-C3	new	14.7	1.12	56.1	377	4.67	8.9	10.40
P254-08-C1	new	14.7	1.44	56.1	512	4.14	7.5	5.39
P254-08-C2	new	14.7	1.44	56.1	512	4.14	7.5	5.39
P254-08-C3	new	14.7	1.44	56.1	512	4.14	7.5	5.39
P254-10-C1	new	14.7	1.44	56.1	512	4.67	8.9	5.96
P254-10-C2	new	14.7	1.44	56.1	512	4.67	8.9	5.96
P254-10-C3	new	14.7	1.44	56.1	512	4.67	8.9	5.96
P254-12-C1	new	14.7	1.44	56.1	512	5.41	11.9	7.95
P254-12-C2	new	14.7	1.44	56.1	512	5.41	11.9	7.95
P254-12-C3	new	14.7	1.44	56.1	512	5.41	11.9	7.95
P268-10-C1	old	14.7	1.80	56.1	510	4.67	8.9	4.80
P268-10-C2	old	14.7	1.80	56.1	510	4.67	8.9	4.80
P268-10-C3	old	14.7	1.80	56.1	510	4.67	8.9	4.80
P268-12-C1	old	14.7	1.80	56.1	510	5.41	11.9	6.41
P268-12-C2	old	14.7	1.80	56.1	510	5.41	11.9	6.41
P268-12-C3	old	14.7	1.80	56.1	510	5.41	11.9	6.41
P297-10-C1	new	14.7	2.52	56.1	475	4.67	8.9	3.68
P297-10-C2	new	14.7	2.52	56.1	475	4.67	8.9	3.68
P297-10-C3	new	14.7	2.52	56.1	475	4.67	8.9	3.68
P297-12-C1	new	14.7	2.52	56.1	475	5.41	11.9	4.92
P297-12-C2	new	14.7	2.52	56.1	475	5.41	11.9	4.92
P297-12-C3	new	14.7	2.52	56.1	475	5.41	11.9	4.92
P397-12-C1	new	17.3	2.52	51.4	475	5.41	11.9	4.54
P397-12-C2	new	17.3	2.52	51.4	475	5.41	11.9	4.54
P397-12-C3	new	17.3	2.52	51.4	475	5.41	11.9	4.54

Appendix C: Sheathing material tests results

The following figures show the load-deformation curves of all sheathing. OSB is shown in Figure C1(a)-(c). Plywood is shown in Figure C1(d)-(f). Gypsum is shown in Figure C1(h)-(i).

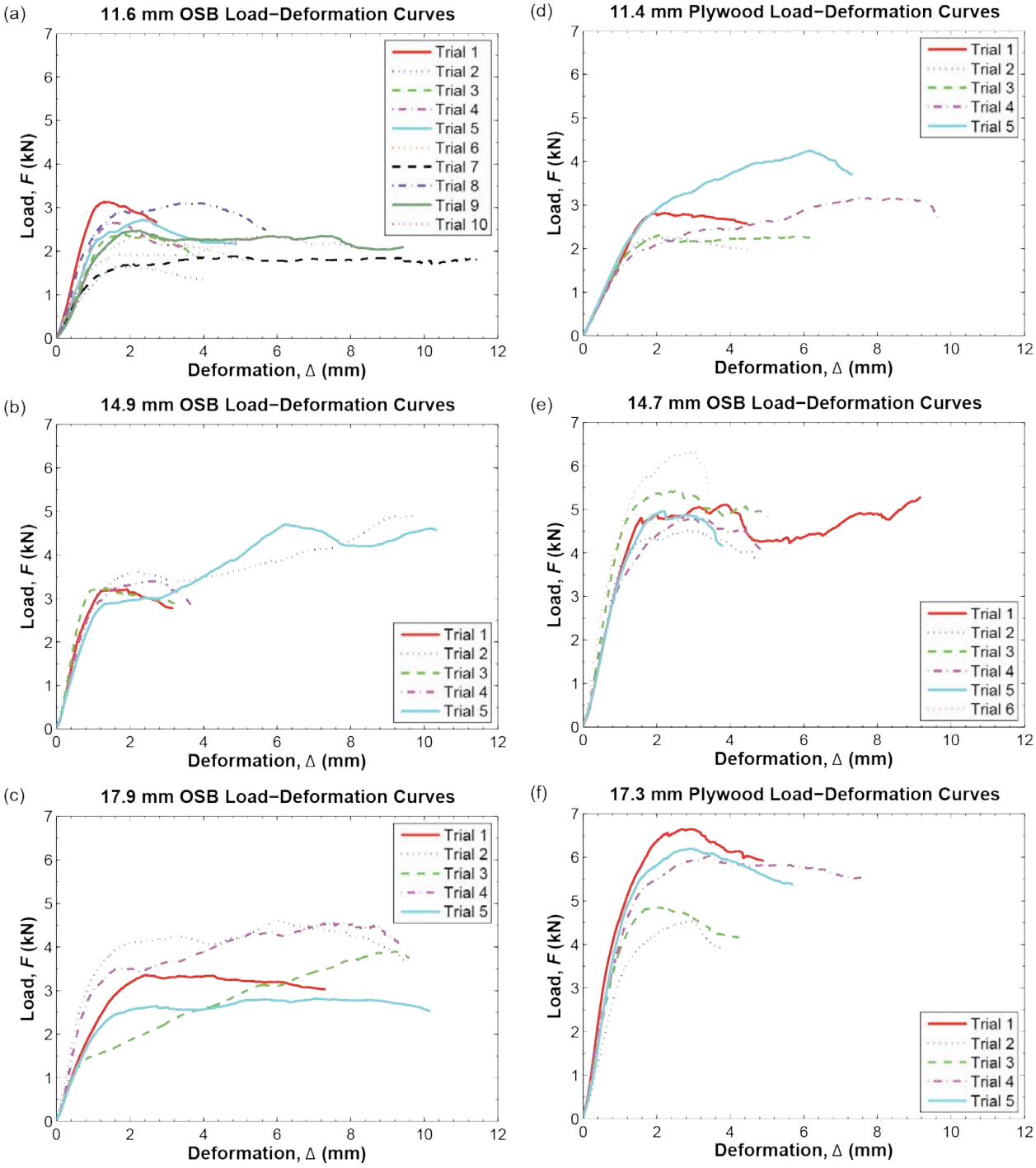

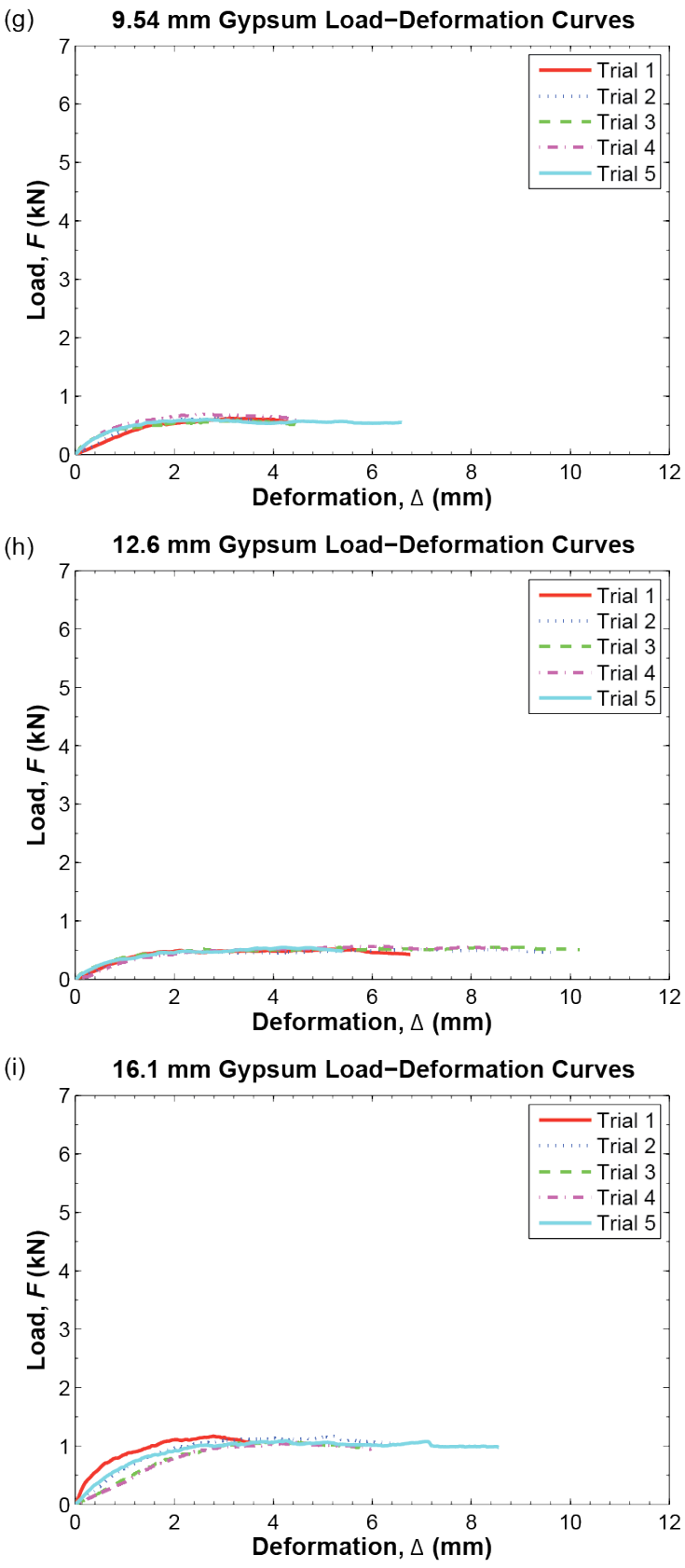

Figure C1: Sheathing stress-strain curves for (a)-(c) OSB, (d)-(f) plywood, (g)-(i) gypsum

Appendix D: Table of backbone parameter values and backbone plots

The following tables contain the backbone parameter values and statistics based on the average of three trials for all the tests. An "*" indicates a fastener shear failure.

Table D1: OSB-to-steel backbone parameter summary and statistics

Test	F_y (kN)		F_c (kN)		F_r (kN)		δ_y (mm)		δ_c (mm)		δ_r (mm)		δ_f (mm)		K_e (kN/mm)		K_s (kN/mm)		K_c (kN/mm)		K_r (kN/mm)	
	μ	c_v	μ	c_v	μ	c_v	μ	c_v	μ	c_v	μ	c_v	μ	c_v	μ	c_v	μ	c_v	μ	c_v	μ	c_v
O133-8-M	1.82	0.25	2.15	0.13	0.87	0.18	1.11	0.07	6.24	0.17	18.82	0.11	63.67	0.04	1.67	0.28	0.06	0.34	-0.11	0.18	-0.02	0.26
O133-8-C+	1.58	0.07	1.94	0.06	1.35	0.05	0.31	0.17	5.30	0.03	12.35	0.09	17.79	0.14	5.19	0.18	0.07	0.19	-0.09	0.16	-0.27	0.28
O233-08-M	1.58	0.15	3.01	0.10	1.36	0.79	1.18	0.44	8.20	0.09	16.89	0.28	48.68	0.55	1.54	0.34	0.20	0.24	-0.19	0.08	-1.84	1.40 *
O233-08-C+	1.22	0.27	2.38	0.09	2.09	0.13	0.21	0.22	6.97	0.40	9.39	0.38	12.56	0.35	5.77	0.10	0.17	0.07	-0.13	0.16	-0.85	0.62 *
O233-10-M	1.72	0.33	2.76	0.11	1.06	0.15	2.06	0.56	10.71	0.13	16.79	0.02	37.60	0.09	0.97	0.39	0.12	0.21	-0.28	0.07	-0.05	0.31
O233-10-C+	1.50	0.24	3.17	0.23	2.20	0.21	0.34	0.20	8.96	0.11	13.03	0.13	21.67	0.14	4.41	0.04	0.19	0.26	-0.23	0.20	-0.26	0.05
O243-08-M	1.92	0.22	3.42	0.08	2.62	0.08	0.95	0.34	8.03	0.28	11.24	0.35	16.77	0.46	2.20	0.27	0.23	0.37	-0.22	0.24	-2.86	1.26 *
O243-08-C+	2.08	0.06	3.10	0.07	1.92	0.46	0.56	0.13	6.97	0.30	9.16	0.28	19.87	0.45	3.80	0.15	0.18	0.38	-0.72	0.91	-1.16	1.08 *
O243-10-M	1.83	0.28	3.63	0.19	1.82	0.09	0.89	0.32	9.64	0.17	15.45	0.06	30.74	0.09	2.17	0.27	0.21	0.20	-0.32	0.24	-0.13	0.25
O243-10-C+	2.00	0.18	3.18	0.11	1.15	0.12	0.36	0.26	5.27	0.37	11.30	0.35	37.27	0.34	5.65	0.07	0.24	0.18	-0.37	0.24	-0.05	0.33
O254-08-M	2.27	0.15	3.55	0.07	1.96	0.08	1.02	0.09	8.06	0.14	14.19	0.05	28.44	0.09	2.25	0.17	0.18	0.14	-0.26	0.26	-0.14	0.14
O254-08-C+	1.75	0.12	2.70	0.13	2.01	0.18	0.47	0.13	9.00	0.04	13.76	0.07	20.20	0.03	3.71	0.05	0.11	0.17	-0.14	0.20	-0.31	0.08
O254-10-M	1.75	0.35	3.64	0.05	1.66	0.19	0.61	0.32	9.72	0.05	18.08	0.09	59.33	0.07	2.85	0.04	0.21	0.22	-0.25	0.30	-0.04	0.24
O254-10-C+	2.17	0.11	3.66	0.08	1.45	0.13	0.47	0.13	8.13	0.18	16.44	0.04	34.87	0.10	4.66	0.15	0.19	0.19	-0.27	0.23	-0.08	0.28
O254-12-M	3.10	0.09	5.03	0.03	2.18	0.20	1.03	0.09	9.99	0.07	22.11	0.03	73.38	0.06	3.00	0.00	0.21	0.17	-0.23	0.07	-0.04	0.12
O254-12-C+	3.08	0.17	3.88	0.12	3.60	0.15	0.53	0.21	7.54	0.22	10.48	0.19	28.97	0.34	5.93	0.06	0.12	0.33	-0.09	0.09	-0.26	0.60
O268-10-M	2.25	0.18	4.21	0.19	2.39	0.15	0.52	0.12	8.37	0.08	16.20	0.06	30.34	0.28	4.28	0.06	0.25	0.14	-0.24	0.29	-0.21	0.47
O268-10-C+	2.00	0.00	3.28	0.07	2.96	0.09	0.32	0.13	8.19	0.02	10.91	0.07	20.59	0.03	6.35	0.12	0.16	0.16	-0.12	0.25	-0.31	0.11
O268-12-M	2.50	0.00	4.51	0.07	2.54	0.09	0.71	0.00	8.95	0.08	18.49	0.14	44.71	0.02	3.50	0.00	0.24	0.08	-0.21	0.04	-0.10	0.10
O268-12-C+	2.17	0.29	4.59	0.07	3.39	0.14	0.27	0.31	9.63	0.04	15.29	0.10	30.57	0.12	8.41	0.17	0.26	0.10	-0.21	0.06	-0.23	0.25
O297-10-M	2.03	0.12	3.27	0.07	2.49	0.15	0.93	0.21	7.30	0.17	10.84	0.26	13.38	0.35	2.23	0.09	0.20	0.14	-0.32	0.70	-1.85	0.59 *
O297-10-C+	2.17	0.05	3.89	0.10	3.53	0.08	0.31	0.29	7.49	0.05	8.34	0.01	9.00	0.00	7.42	0.22	0.24	0.15	-0.50	0.42	-5.53	0.23 *
O297-12-M	2.75	0.22	4.69	0.08	3.62	0.14	0.77	0.25	8.30	0.25	11.65	0.10	19.74	0.28	3.58	0.03	0.28	0.34	-0.33	0.11	-4.53	1.33 *
O297-12-C+	3.33	0.19	5.42	0.11	3.80	0.07	0.50	0.30	7.81	0.24	11.75	0.05	15.17	0.13	6.96	0.12	0.31	0.24	-0.72	0.71	-1.37	0.48 *
O397-12-M	2.08	0.46	4.56	0.29	3.28	0.35	0.77	0.55	11.76	0.11	17.92	0.14	19.19	0.15	3.00	0.24	0.24	0.36	-0.16	0.45	-2.62	0.34 *
O397-12-C+	3.92	0.13	5.08	0.07	3.72	0.22	0.42	0.28	8.84	0.18	14.24	0.15	15.50	0.11	9.75	0.20	0.14	0.27	-0.28	0.73	-3.07	0.27 *

Table D2: Plywood-to-steel backbone parameter summary and statistics

Test	F_y (kN)		F_c (kN)		F_r (kN)		δ_y (mm)		δ_c (mm)		δ_r (mm)		δ_f (mm)		K_e (kN/mm)		K_s (kN/mm)		K_c (kN/mm)		K_r (kN/mm)	
	μ	c_v	μ	c_v	μ	c_v	μ	c_v	μ	c_v	μ	c_v	μ	c_v	μ	c_v	μ	c_v	μ	c_v	μ	c_v
P133-8-M	1.18	0.11	1.89	0.09	1.17	0.07	0.37	0.11	9.88	0.17	16.17	0.09	30.77	0.26	3.17	0.07	0.07	0.33	-0.13	0.49	-0.10	0.42
P133-8-C+	1.30	0.11	2.03	0.13	0.58	0.12	0.45	0.33	7.74	0.14	16.86	0.01	44.14	0.01	3.12	0.27	0.10	0.13	-0.17	0.35	-0.02	0.13
P233-08-M	1.55	0.09	3.41	0.05	2.17	0.10	0.52	0.32	8.86	0.11	13.69	0.09	21.50	0.19	3.25	0.27	0.22	0.07	-0.27	0.29	-0.34	0.49
P233-08-C+	1.58	0.07	2.35	0.06	0.67	0.17	0.47	0.09	4.21	0.27	6.29	0.21	10.73	0.13	3.40	0.04	0.20	0.09	-1.07	0.57	-0.16	0.30 *
P233-10-M	1.33	0.35	3.62	0.18	1.38	0.16	0.78	0.20	10.48	0.09	18.76	0.12	45.08	0.10	1.67	0.14	0.24	0.09	-0.29	0.42	-0.05	0.19
P233-10-C+	1.67	0.07	3.83	0.03	2.04	0.02	0.56	0.24	10.45	0.06	17.19	0.05	26.89	0.06	3.10	0.18	0.22	0.07	-0.28	0.28	-0.21	0.06
P243-08-M	1.30	0.25	2.96	0.10	1.16	0.31	0.82	0.16	7.19	0.42	12.10	0.47	23.16	0.56	1.67	0.37	0.28	0.15	-0.54	0.60	-0.19	0.64 *
P243-08-C+	2.00	0.10	3.47	0.12	1.15	0.45	0.43	0.20	7.92	0.48	10.45	0.48	20.25	0.11	4.79	0.11	0.25	0.42	-1.91	0.62	-0.14	0.47 *
P243-10-M	2.13	0.24	4.13	0.21	1.23	0.26	1.53	0.29	10.59	0.16	23.05	0.06	52.40	0.04	1.42	0.08	0.22	0.18	-0.25	0.37	-0.04	0.30
P243-10-C+	2.00	0.20	4.08	0.02	1.78	0.29	0.47	0.35	8.36	0.07	15.85	0.22	27.30	0.34	4.64	0.26	0.26	0.12	-0.34	0.28	-0.21	0.44
P254-08-M	2.00	0.20	4.14	0.04	1.19	0.24	0.74	0.14	9.69	0.12	18.98	0.02	28.35	0.15	2.67	0.09	0.24	0.21	-0.32	0.16	-0.15	0.43
P254-08-C+	2.00	0.10	3.86	0.03	1.50	0.17	0.34	0.25	6.50	0.29	10.97	0.44	15.75	0.32	6.21	0.23	0.33	0.27	-0.87	0.60	-0.41	0.48 *
P254-10-M	2.67	0.12	3.49	0.15	2.16	0.11	1.29	0.16	11.70	0.11	17.06	0.04	44.74	0.17	2.08	0.06	0.08	0.38	-0.26	0.35	-0.08	0.27
P254-10-C+	2.08	0.15	4.38	0.06	1.23	0.09	0.41	0.11	9.11	0.02	18.86	0.08	25.17	0.17	5.10	0.06	0.26	0.18	-0.33	0.17	-0.23	0.39
P254-12-M	3.40	0.13	6.11	0.09	3.54	0.16	1.27	0.04	12.64	0.07	21.85	0.04	37.69	0.03	2.67	0.09	0.24	0.24	-0.28	0.07	-0.22	0.11
P254-12-C+	3.17	0.23	4.93	0.10	1.98	0.01	0.49	0.19	9.87	0.16	23.44	0.07	34.90	0.08	6.39	0.06	0.20	0.35	-0.23	0.26	-0.21	0.45
P268-10-M	3.08	0.04	5.43	0.05	1.79	0.11	1.03	0.04	9.87	0.11	21.20	0.03	32.80	0.11	3.00	0.00	0.27	0.19	-0.32	0.05	-0.17	0.42
P268-10-C+	2.58	0.05	4.51	0.02	2.31	0.06	0.59	0.15	9.92	0.03	15.96	0.00	20.88	0.08	4.44	0.13	0.21	0.05	-0.37	0.14	-0.51	0.25
P268-12-M	4.50	0.09	6.20	0.03	2.62	0.10	1.92	0.23	13.31	0.07	26.47	0.13	42.28	0.11	2.42	0.13	0.15	0.25	-0.28	0.19	-0.17	0.12
P268-12-C+	3.17	0.07	5.50	0.14	3.70	0.11	0.47	0.33	10.87	0.20	17.33	0.12	27.15	0.16	7.29	0.24	0.22	0.10	-0.28	0.57	-0.49	0.46
P297-10-M	2.67	0.12	4.68	0.08	3.39	0.13	0.85	0.13	7.56	0.12	11.87	0.19	12.84	0.19	3.17	0.13	0.30	0.25	-0.39	0.52	-3.77	0.33 *
P297-10-C+	3.00	0.14	4.78	0.07	2.42	0.49	0.40	0.09	6.05	0.23	7.15	0.17	8.10	0.16	7.74	0.23	0.33	0.20	-4.20	0.63	-2.54	0.32 *
P297-12-M	3.67	0.31	6.18	0.17	4.89	0.19	1.01	0.34	8.74	0.20	15.04	0.07	17.13	0.10	3.67	0.03	0.32	0.18	-0.21	0.16	-4.10	0.69 *
P297-12-C+	4.00	0.00	6.46	0.06	5.25	0.17	0.71	0.23	11.16	0.21	13.18	0.12	15.87	0.19	5.95	0.23	0.25	0.25	-1.22	1.09	-3.04	0.56 *
P397-12-M	4.00	0.00	7.67	0.03	5.76	0.16	1.00	0.00	13.76	0.12	20.47	0.11	22.33	0.11	4.00	0.00	0.29	0.08	-0.29	0.17	-3.14	0.23 *
P397-12-C+	4.33	0.05	7.53	0.02	6.30	0.09	0.51	0.14	11.89	0.06	18.24	0.03	20.00	0.04	8.75	0.18	0.28	0.03	-0.19	0.36	-4.40	0.51 *

Table D3: Steel-to-steel backbone parameter summary and statistics

Test	F_y (kN)		F_c (kN)		F_r (kN)		δ_y (mm)		δ_c (mm)		δ_r (mm)		δ_f (mm)		K_e (kN/mm)		K_s (kN/mm)		K_c (kN/mm)		K_r (kN/mm)	
	μ	c_v	μ	c_v	μ	c_v	μ	c_v	μ	c_v	μ	c_v	μ	c_v	μ	c_v	μ	c_v	μ	c_v	μ	c_v	
2654-8-M	1.60	0.06	2.41	0.08	1.24	0.04	0.29	0.30	2.60	0.04	15.33	0.20	30.30	0.01	6.04	0.28	0.35	0.20	-0.10	0.17	-0.09	0.21	
2654-8-C+	1.93	0.13	2.36	0.13	1.40	0.17	0.10	0.25	2.13	0.24	11.49	0.25	33.28	0.17	20.63	0.15	0.24	0.43	-0.11	0.30	-0.07	0.28	
2654-10-M	1.63	0.21	2.28	0.09	1.21	0.34	0.68	0.19	3.01	0.08	30.13	0.28	54.94	0.13	2.61	0.43	0.29	0.30	-0.04	0.19	-0.05	0.32	
2654-10-C+	1.42	0.08	2.17	0.05	1.76	0.08	0.34	0.10	2.44	0.33	22.11	0.14	32.01	0.16	4.17	0.14	0.46	0.57	-0.02	0.14	-0.20	0.37	
2654-12-M	2.00	0.18	2.75	0.08	1.65	0.09	0.72	0.27	2.29	0.19	9.45	0.07	52.92	0.09	2.92	0.26	0.50	0.14	-0.15	0.28	-0.04	0.07	
2654-12-C+	1.48	0.04	2.00	0.14	1.51	0.11	0.44	0.34	3.26	0.36	11.95	0.13	43.30	0.26	3.92	0.39	0.18	0.23	-0.06	0.33	-0.05	0.22	
3333-8-M	2.18	0.06	2.96	0.03	1.90	0.08	0.67	0.35	4.01	0.15	12.16	0.11	23.25	0.13	3.62	0.28	0.25	0.34	-0.14	0.22	-0.18	0.21	
3333-8-C+	1.90	0.19	3.53	0.08	1.71	0.07	0.39	0.64	4.75	0.11	10.36	0.05	23.72	0.06	6.70	0.50	0.39	0.36	-0.33	0.14	-0.13	0.15	
3333-10-M	2.12	0.13	2.93	0.02	1.84	0.09	0.80	0.77	6.33	0.15	15.26	0.04	30.53	0.04	5.15	0.69	0.16	0.44	-0.12	0.13	-0.12	0.12	
3333-10-C+	2.35	0.11	3.50	0.06	1.83	0.18	0.55	0.42	5.61	0.20	12.13	0.21	19.82	0.22	5.11	0.41	0.25	0.58	-0.32	0.43	-0.28	0.39	
3333-12-M	2.71	0.02	3.16	0.03	2.16	0.09	0.82	0.54	8.40	0.04	14.37	0.05	30.08	0.06	4.20	0.40	0.06	0.39	-0.17	0.21	-0.14	0.18	
3333-12-C+	2.24	0.04	3.23	0.15	2.20	0.10	0.74	0.54	5.18	0.35	10.45	0.01	16.65	0.22	5.08	0.77	0.24	0.28	-0.24	0.74	-0.56	0.69	
4333-8-M	2.58	0.20	4.53	0.03	3.59	0.13	0.78	0.74	4.39	0.06	5.04	0.11	5.34	0.14	4.72	0.40	0.53	0.21	-2.06	0.68	-15.19	0.36	*
4333-8-C+	2.58	0.12	4.35	0.17	4.19	0.20	0.22	0.22	4.16	0.43	5.84	0.09	6.87	0.16	13.00	0.38	0.55	0.43	-0.25	0.70	-7.22	0.63	*
4333-10-M	3.00	0.24	4.78	0.03	2.23	0.24	1.32	0.37	6.85	0.08	9.93	0.03	21.29	0.27	2.39	0.15	0.31	0.34	-0.85	0.25	-0.29	0.60	
4333-10-C+	3.00	0.07	3.79	0.08	3.14	0.16	0.55	0.33	6.23	0.16	11.12	0.11	12.81	0.10	5.96	0.27	0.14	0.15	-0.14	0.54	-1.87	0.19	
4333-12-M	2.92	0.04	5.43	0.04	3.03	0.04	1.45	0.37	9.25	0.14	14.09	0.13	34.62	0.22	2.29	0.33	0.33	0.11	-0.49	0.01	-0.20	0.57	
4333-12-C+	3.32	0.14	4.74	0.17	3.16	0.21	1.21	0.35	5.91	0.49	13.95	0.17	24.93	0.03	3.23	0.48	0.31	0.08	-0.22	0.63	-0.29	0.14	
4343-8-M	3.21	0.12	4.95	0.02	3.76	0.09	0.26	0.51	2.96	0.08	3.86	0.14	4.48	0.17	18.70	0.66	0.65	0.23	-1.50	0.50	-7.53	0.51	*
4343-8-C+	2.59	0.14	4.91	0.06	3.45	0.23	0.16	0.29	3.41	0.41	5.66	0.22	6.62	0.19	17.36	0.16	0.79	0.34	-0.69	0.82	-8.06	1.01	*
4343-10-M	4.67	0.05	5.47	0.04	2.89	0.16	1.15	0.26	4.97	0.18	14.10	0.21	26.26	0.07	4.39	0.29	0.21	0.18	-0.30	0.13	-0.26	0.28	
4343-10-C+	3.36	0.07	5.79	0.03	3.31	0.09	0.48	0.18	4.53	0.29	9.41	0.16	13.87	0.13	7.23	0.17	0.66	0.32	-0.62	0.48	-0.85	0.36	
4343-12-M	4.75	0.11	5.70	0.04	3.18	0.10	0.80	0.39	3.70	0.19	13.20	0.08	25.83	0.05	7.07	0.41	0.29	0.45	-0.26	0.18	-0.26	0.13	
4343-12-C+	4.07	0.18	6.48	0.03	2.77	0.36	0.21	0.49	2.22	0.23	11.07	0.26	17.92	0.18	21.73	0.26	1.26	0.21	-0.42	0.12	-0.41	0.31	
4354-8-M	4.58	0.13	5.81	0.10	4.42	0.20	0.37	0.31	3.77	0.54	4.91	0.59	10.97	1.01	14.12	0.37	0.48	0.44	-1.52	0.40	-18.31	0.89	*
4354-8-C+	4.48	0.09	5.41	0.05	4.93	0.08	0.12	0.17	1.52	0.34	3.14	0.38	3.55	0.40	38.83	0.10	0.73	0.25	-0.92	1.19	-17.12	0.59	*
4354-10-M	4.58	0.07	7.03	0.05	4.12	0.05	0.87	0.40	6.93	0.09	13.47	0.04	24.17	0.05	6.18	0.39	0.41	0.24	-0.46	0.23	-0.39	0.16	
4354-10-C+	4.74	0.05	5.69	0.01	5.34	0.02	0.49	0.08	2.30	0.07	7.50	0.03	13.32	0.07	9.70	0.08	0.53	0.18	-0.07	0.31	-0.94	0.16	*
4354-12-M	6.08	0.02	6.96	0.02	4.28	0.21	0.64	0.74	4.39	0.39	12.91	0.13	24.42	0.08	15.08	0.51	0.26	0.27	-0.36	0.56	-0.39	0.27	
4354-12-C+	4.42	0.07	6.66	0.01	5.87	0.05	0.20	0.00	2.33	0.06	6.74	0.11	10.06	0.13	22.08	0.07	1.06	0.19	-0.18	0.21	-2.45	0.49	
4368-8-M	5.72	0.07	6.93	0.03	5.42	0.10	0.26	0.25	1.31	0.20	1.76	0.23	1.89	0.22	23.32	0.23	1.16	0.23	-3.96	0.45	-41.55	0.16	*
4368-8-C+	5.75	0.04	6.76	0.03	5.82	0.09	0.24	0.16	1.37	0.15	1.67	0.10	1.95	0.10	24.94	0.17	0.90	0.10	-3.73	0.54	-21.51	0.14	*
4368-10-M	5.69	0.14	8.83	0.07	4.64	0.08	0.75	0.25	11.39	0.01	14.48	0.10	25.84	0.04	8.19	0.30	0.30	0.41	-1.72	0.40	-0.42	0.16	
4368-10-C+	3.90	0.14	7.97	0.01	4.41	0.54	0.38	0.06	7.41	0.12	10.39	0.09	15.39	0.20	10.38	0.18	0.58	0.06	-1.05	0.26	-1.22	0.75	*
4368-12-M	7.00	0.00	8.29	0.01	6.86	0.07	0.59	0.12	2.90	0.07	14.54	0.01	28.25	0.10	12.06	0.12	0.57	0.11	-0.12	0.34	-0.52	0.13	
4368-12-C+	5.42	0.02	8.73	0.04	4.65	0.09	0.28	0.21	8.02	0.13	12.90	0.01	13.91	0.03	20.47	0.25	0.44	0.18	-0.88	0.20	-5.03	0.36	
4397-8-M	5.25	0.10	6.78	0.02	5.40	0.04	0.26	0.13	1.18	0.41	1.62	0.30	1.88	0.28	20.72	0.15	1.80	0.30	-3.30	0.19	-25.54	0.48	*
4397-8-C+	5.83	0.04	7.07	0.01	6.26	0.05	0.14	0.20	0.74	0.13	1.04	0.14	1.36	0.13	41.77	0.16	2.10	0.07	-3.26	0.48	-21.55	0.30	*
4397-10-M	6.10	0.08	10.44	0.08	8.83	0.25	0.89	0.27	8.49	0.12	10.45	0.27	10.92	0.27	7.31	0.26	0.56	0.17	-1.97	0.98	-27.83	0.60	*
4397-10-C+	4.66	0.20	6.95	0.05	6.33	0.05	0.08	0.20	1.42	0.18	8.26	0.17	10.09	0.25	63.23	0.41	1.74	0.29	-0.09	0.13	-7.18	0.86	*
4397-12-M	7.73	0.03	12.56	0.02	9.75	0.13	1.12	0.07	9.53	0.06	26.98	0.09	54.62	0.15	6.91	0.05	0.58	0.07	-0.17	0.61	-0.43	0.55	
4397-12-C+	9.00	0.00	11.34	0.08	7.48	0.03	0.72	0.12	12.36	0.08	26.27	0.23	44.99	0.20	12.75	0.13	0.20	0.36	-0.38	0.61	-0.42	0.22	
5426-8-M	1.03	0.12	1.26	0.13	1.01	0.10	1.09	0.27	3.91	0.30	28.19	0.14	43.61	0.09	1.01	0.24	0.10	0.50	-0.01	0.32	-0.08	0.45	
5426-8-C+	1.03	0.16	1.48	0.16	1.15	0.11	0.19	0.35	20.94	0.31	26.40	0.16	35.42	0.09	6.18	0.44	0.02	0.33	-0.06	0.23	-0.13	0.28	
5426-10-M	0.94	0.08	1.15	0.09	0.91	0.08	0.54	0.29	1.63	0.33	35.19	0.04	52.33	0.06	1.92	0.35	0.20	0.45	-0.01	0.21	-0.05	0.23	
5426-10-C+	1.03	0.12	1.51	0.13	1.14	0.10	0.25	0.17	3.63	0.40	15.31	0.13	32.45	0.11	4.23	0.22	0.17	0.39	-0.03	0.32	-0.07	0.21	
5426-12-M	1.00	0.04	1.34	0.05	1.08	0.02	0.78	0.16	4.90	0.28	29.46	0.04	46.54	0.04	1.33	0.19	0.10	0.45	-0.01	0.23	-0.07	0.15	
5426-12-C+	0.97	0.13	1.32	0.03	0.93	0.09	0.18	0.35	5.13	0.25	20.15	0.13	38.82	0.11	5.81	0.24	0.07	0.33	-0.03	0.13	-0.05	0.21	
5433-8-M	2.52	0.05	4.38	0.05	3.25	0.10	0.82	0.07	5.54	0.05	5.91	0.06	6.39	0.07	3.11	0.10	0.40	0.20	-3.27	0.20	-7.39	0.35	*
5433-8-C+	2.92	0.11	4.34	0.04	3.97	0.06	0.13	0.32	4.94	0.21	6.59	0.15	6.99	0.16	24.51	0.27	0.29	0.12	-0.59	0.67	-17.92	0.75	*
5433-10-M	2.97	0.01	5.16	0.02	3.04	0.16	0.60	0.30	5.17	0.10	8.33	0.17	25.18	0.15	5.48	0.33	0.48	0.02	-0.69	0.12	-0.19	0.28	
5433-10-C+	2.92	0.04	4.84	0.05	2.45	0.09	0.08	0.17	5.75	0.11	13.32	0.24	19.64	0.17	36.98	0.13	0.35	0.23	-0.40	0.55	-0.61	0.69	
5433-12-M	3.04	0.07	5.69	0.03	3.45	0.20	0.80	0.50	8.34	0.17	13.14	0.23	35.48	0.07	5.17	0.56	0.36	0.19	-0.48	0.17	-0.16	0.05	
5433-12-C+	2.83	0.08	5.48	0.01	2.90	0.25	0.12	0.20	11.38	0.05	18.77	0.16	37.84	0.22	25.00	0.16	0.24	0.12	-0.41	0.33	-0.19	0.43	
6833-8-M	2.92	0.11	4.14	0.01	3.11	0.18	0.09	0.56	4.25	0.11	5.94	0.31	9.37	0.62	43.21	0.46	0.29	0.16	-0.83	0.61	-3.87	0.66	*
6833-8-C+	2.97	0.06	3.97	0.05	2.84	0.33	0.13	0.31	5.64	0.17	8.48	0.53	9.87	0.46	25.50	0.29	0.20	0.37	-1.84	0.67	-16.44	1.30	*
6833-10-M	4.00	0.00	4.98	0.07	2.87	0.21	1.95	0.13	4.97	0.13	8.77	0.14	21.88	0.18	2.09	0.14	0.33	0.36	-0.55	0.23	-0.24	0.45	
6833-10-C+	3.42	0.07	4.67	0.07	2.90	0.07	0.20	0.00	4.71	0.18	9.86	0.13	15.24	0.05	17.08	0.07	0.29	0.30	-0.35	0.13	-0.54	0.07	
6833-12-M	3.44	0.09	4.74	0.06	3.21	0.08	1.10	0.49	5.81	0.20	16.20	0.08	35.26	0.14	3.74	0.34	0.30	0.47	-0.15	0.13	-0.18	0.20	
6833-12-C+	3.17	0.19	4.40	0.04	3.09	0.05	0.09	0.19	6.33	0.26	18.29	0.03	24.48	0.14	34.99	0.20	0.19	0.37	-0.11	0.12	-0.79	0.68	
9733-8-M	1.42	0.81	1.76	0.80	1.15	0.70	0.31	0.14	1.90	0.95	2.52	0.78	3.40	0.52	5.23	0.93	0.41	0.45	-0.81	0.94	-1.75	0.82	*
9733-8-C+	2.65	0.12	4.05	0.10	3.58	0.25	0.07	0.32	3.11	0.27	3.47	0.15	3.63	0.16	41.32	0.24	0.45	0.10	-1.13	0.60	-26.00	0.32	*
9733-10-M	3.33	0.04	4.12	0.05	2.54	0.01	1.68	0.17	5.09	0.32	10.39	0.14	21.48	0.11	2.05	0.19	0.28	0.42	-0.32	0.32	-0.23	0.14	
9733-10-C+	2.67	0.04	4.49	0.08	2.07	0.34	0.04	0.23	6.23	0.03	11.47	0.13	14.44	0.09	73.91	0.24	0.29	0.22	-0.44	0.27	-1.16	0.45	
9733-12-M	3.36	0.06	4.80	0.06	3.63	0.02	0.80	0.29	2.88	0.04	13.71	0.06	35.02	0.11	4.61	0.32	0.70	0.10	-0.11	0.20	-0.17	0.15	
9733-12-C+	2.89	0.19	4.64	0.06	3.24	0.18	0.25	0.53	3.04	0.10	18.88	0.13	24.15	0.02	16.00	0.62	0.62	0.07	-0.09	0.20	-0.73	0.38	
9768-10-M	3.83	0.22	6.70	0.03	5.82	0.05	0.06	0.44	0.96	0.09	1.49	0.07	1.89	0.06	67.76	0.23	3.19	0.32	-1.64	0.26	-19.40	0.50	*
9768-10-C+	4.33	0.29	6.29	0.06	5.22	0.19	0.21	0.40	0.71	0.25	1.03	0.31	1.35	0.24	23.26	0.36	3.64	0.19	-2.84	0.39	-17.98	0.33	*
9768-12-M	6.83	0.15	9.74	0.06	8.70	0.05	0.37	0.46	2.27	0.30	2.65	0.26	2.99	0.17	23.61	0.49	1.70	0.44	-2.66	0.27	-39.39	0.69	*
9768-12-C+	6.67	0.07	9.79	0.06	8.70	0.13	0.31	0.24	2.04	0.12	2.30	0.10	2.63	0.11	22.41	0.21	1.81	0.01	-4.64	0.27	-26.65	0.20	*
9797-10-M	5.50	0.07	7.36	0.03	5.19	0.08	0.13	0.08	0.64	0.15	1.23	0.11	1.47	0.08	43.33	0.14	3.67	0.17	-3.73	0.05	-22.05	0.13	*
9797-10-C+	4.50	0.24	7.17	0.01	5.56	0.08	0.09	0.23	0.63	0.41	0.84	0.31	1.16	0.14	53.28	0.45	5.44	0.33	-9.94	0.35	-19.97	0.40	*
9797-12-M	7.00	0.12	10.91	0.03	9.56	0.08	0.19	0.14	1.69	0.11	1.98	0.08	2.09	0.08	36.67	0.06	2.65	0.19	-4.50	0.24	-90.47	0.18	*
9797-12-C+	7.67	0.06	10.79	0.04	9.83	0.06	0.25	0.45	1.59	0.13	1.74	0.16	2.59	0.19	37.52	0.40	2.41	0.18	-7.90	0.36	-16.03	0.44	*

Table D4: Gypsum-to-steel backbone parameter summary and statistics

Test	F_y (kN)		F_c (kN)		F_r (kN)		δ_y (mm)		δ_c (mm)		δ_r (mm)		δ_f (mm)		K_e (kN/mm)		K_s (kN/mm)		K_c (kN/mm)		K_r (kN/mm)	
	μ	c_v	μ	c_v	μ	c_v	μ	c_v	μ	c_v	μ	c_v	μ	c_v	μ	c_v	μ	c_v	μ	c_v	μ	c_v
G133-6-M	0.61	0.02	0.69	0.01	0.36	0.01	1.55	0.03	6.46	0.17	24.90	0.06	40.73	0.07	0.31	0.03	0.02	0.18	-0.02	0.03	-0.02	0.16
G133-6-C+	0.48	0.05	0.60	0.04	0.35	0.13	0.87	0.13	4.25	0.26	21.09	0.07	32.76	0.11	1.08	0.09	0.04	0.20	-0.01	0.11	-0.03	0.27
G233-6-M	0.41	0.10	0.51	0.04	0.32	0.13	1.29	0.07	8.28	0.14	25.01	0.19	50.20	0.01	0.33	0.08	0.02	0.18	-0.01	0.06	-0.01	0.08
G233-6-C+	0.37	0.03	0.46	0.02	0.36	0.07	0.34	0.08	11.02	0.18	21.54	0.17	34.71	0.18	0.84	0.11	0.01	0.19	-0.01	0.28	-0.03	0.26
G243-6-M	0.43	0.05	0.50	0.04	0.41	0.06	1.34	0.15	10.55	0.41	25.10	0.03	31.36	0.05	0.43	0.19	0.01	0.29	-0.01	0.19	-0.07	0.26
G243-6-C+	0.34	0.19	0.52	0.13	0.42	0.09	0.41	0.21	10.41	0.10	18.44	0.11	41.98	0.12	0.82	0.04	0.02	0.11	-0.01	0.23	-0.02	0.19
G254-6-M	0.42	0.03	0.57	0.03	0.47	0.04	0.97	0.02	9.96	0.29	24.09	0.11	29.50	0.03	0.71	0.05	0.02	0.31	-0.01	0.32	-0.10	0.33
G254-6-C+	0.42	0.03	0.53	0.01	0.41	0.09	0.54	0.24	9.27	0.01	26.07	0.02	36.77	0.06	1.18	0.26	0.01	0.09	-0.01	0.25	-0.04	0.27
G354-6-M	0.87	0.03	1.04	0.03	0.54	0.42	1.23	0.01	8.91	0.23	14.15	0.16	17.40	0.19	0.00	0.02	0.03	0.36	-0.09	0.45	-0.22	0.76 *
G354-6-C+	0.65	0.06	0.86	0.04	0.27	1.07	0.56	0.16	6.96	0.02	8.68	0.12	11.29	0.07	0.00	0.09	0.03	0.23	-0.50	0.63	-0.56	1.37 *

The load-deformation data, backbone values, and plots of the backbones on the load-deformation data are available online at:

https://drive.google.com/folderview?id=0B5bYeCZjlFbDYm4wcFJPZ3U4TkU&usp=sharing

Files are organized by material type (steel, OSB, plywood, and gypsum), loading type (monotonic and cyclic), ply combination, and trial number. Each folder contains 4 files: two text files, one .mat (Matlab data) file, and one PDF file. Within the .mat file, there are four vectors: load (kN), displacement (mm), load data points of the backbone (kN), and displacement data points of the backbone (mm). The “Backbone_Data” text file contains the load and displacement data points of the backbone in CSV format, with the first column as the displacement values (mm) and the second column as the load values (kN). The “LoadDisp_Data” text file contains the raw load and displacement values in CSV format, with the first column as the displacement values (mm) and the second column as the load values (kN). The PDF file is a Matlab plot of the backbone and raw load-deformation response.

American Iron and Steel Institute

25 Massachusetts Avenue, NW
Suite 800
Washington, DC 20001

www.steel.org

Research Report RP17-2

The New Steel